The snoGloBe interaction predictor reveals a broad spectrum of C/D snoRNA RNA targets

Running title: snoGloBe: an accurate predictor of C/D snoRNA interactions

Gabrielle Deschamps-Francoeur[1], Sonia Couture[2], Sherif Abou-Elela[2], Michelle S. Scott[1,*]

[1] Département de biochimie et de génomique fonctionnelle, Faculté de médecine et des sciences de la santé, Université de Sherbrooke, Sherbrooke, Québec, J1E 4K8, Canada

[2] Département de microbiologie et d'infectiologie, Faculté de médecine et des sciences de la santé, Université de Sherbrooke, Sherbrooke, Québec, J1E 4K8, Canada

* Corresponding author: michelle.scott@usherbrooke.ca

Keywords: snoRNA, RNA target prediction, RNA-RNA duplex, gradient boosting classifier, RNA-seq, RNA stability, alternative splicing regulation

ABSTRACT

Box C/D small nucleolar RNAs (snoRNAs) are a conserved class of RNA known for their role in guiding ribosomal RNA 2'-O-ribose methylation through base pairing with targeted sequences. Recently, C/D snoRNAs were also implicated in regulating the expression of non-ribosomal genes through different modes of binding. Large scale RNA-RNA interaction datasets detect many snoRNAs binding messenger RNA. However, these studies provide a narrow portrait of snoRNA targets forming under specific experimental conditions. To enable a more comprehensive study of C/D snoRNA interactions, we created snoGloBe, a human C/D snoRNA machine learning interaction predictor based on a gradient boosting classifier. SnoGloBe considers the target type, and position and sequence of the interactions, enabling it to outperform existing predictors. Interestingly, for specific snoRNAs, snoGloBe identifies strong enrichment of interactions near gene expression regulatory elements including splice sites. Abundance and splicing of predicted targets were altered upon the knockdown of their associated snoRNA. Strikingly, the predicted snoRNA interactions often overlap with the binding sites of functionally related RNA binding proteins, reinforcing their role in gene expression regulation. The interactions of snoRNAs are not randomly distributed but often accumulate in functionally related transcripts sharing common regulatory elements suggesting coordinated regulatory function. The wide scope of snoGloBe makes it an excellent tool for discovering viral RNA targets, which is evident from its capacity to identify snoRNAs targeting SARS-CoV-2 RNA, known to be heavily methylated. Overall, snoGloBe is capable of identifying experimentally validated binding sites and predicting novel sites with shared regulatory function.

INTRODUCTION

Small nucleolar RNAs (snoRNAs) are a conserved class of noncoding RNA required for rRNA modification, processing, and assembly (Maxwell and Fournier 1995). In addition, snoRNAs contribute to spliceosome biogenesis by guiding the modification of small nuclear RNA (snRNA) (Kiss 2001). To carry out these functions, deemed canonical, they assemble in ribonucleoprotein (snoRNP) complexes which provide them stability and catalytic activity. SnoRNAs are split in two families based on their structure, conserved motifs, interacting proteins and modification type. Box C/D snoRNAs guide 2'-O-ribose methylation while box H/ACA snoRNAs guide pseudouridylation of RNA (Kiss-László et al. 1996; Ganot et al. 1997). SnoRNAs of both families identify their modification targets through base pairing between the snoRNA guide sequence and the sequence flanking the modification sites (Weinstein and Steitz 1999).

Box C/D snoRNAs usually range between 50-100 nucleotides in length and are characterized by their conserved motifs: the boxes C/C' (RUGAUGA) and D/D' (CUGA) (Figure 1A). They interact with core binding proteins SNU13, NOP56, NOP58 and the methyltransferase fibrillarin (FBL) to form the C/D snoRNP. Box C/D snoRNAs guide their catalytic partner to the modification site using sequence complementarity to the region upstream of the boxes D and D', called the antisense element (ASE) (Kiss-László et al. 1996; Chen et al. 2007). Box C/D snoRNA ASEs range between 10 and 20 nucleotides in length and are deemed essential for rRNA modification. However, many C/D snoRNAs have no identified canonical modification target and are referred to as orphan snoRNAs. Interestingly, some snoRNAs were also described as guiding the modification of messenger RNAs (mRNAs) expanding the confines of potential RNA targets (Elliott et al. 2019).

In recent years, a wide range of functions have been discovered for box C/D snoRNAs, including the regulation of chromatin compaction, metabolic stress, cholesterol trafficking, alternative splicing and mRNA levels (reviewed in (Dupuis-Sandoval et al. 2015; Falaleeva et al. 2017; Bratkovič et al. 2020)). These functions are often mediated by noncanonical pairing configurations with the interactions involving diverse regions of the snoRNA sequence (Figure 1B). As such, complementarity to the ASE employed for methylation cannot be used as sole indicator of potential noncanonical targets. In this paper, we define a canonical interaction as an interaction leading to the methylation of a rRNA or a snRNA, and all others are defined as noncanonical, including interactions leading to the methylation of other types of RNA such as mRNA and transfer RNA (tRNA).

Genome wide methods for detecting RNA-RNA interactions identified a large number of noncanonical snoRNA interactions. These methods, including PARIS (Lu et al. 2016), LIGR-seq (Sharma et al. 2016) and SPLASH (Aw et al. 2016), have been devised to survey all RNA duplexes in cells, both intra- and intermolecular. They have enabled the detection of known and novel snoRNA interactions. For example, LIGR-seq identified functional interactions between orphan snoRNA SNORD83B and three different mRNAs affecting their stability (Sharma et al. 2016). Indeed, these large-scale experimental approaches play an important role in uncovering noncanonical snoRNA targets. However, these methods are limited by cell type, growth conditions and cross-linking approach used to produce the data. In addition, they often suffer from low proportion of intermolecular duplex reads (Schönberger et al. 2018) and consequently reduced coverage of snoRNA interactions, which form a relatively small proportion of all possible interactions in the human transcriptome, suggesting that there are probably plenty of snoRNA-RNA interactions yet to uncover.

In silico prediction of snoRNA interactions has the potential to uncover all possible transcriptome-wide snoRNA interactions since they are not restricted by experimental constraints. However, available RNA-RNA interaction prediction tools are often built on known mechanisms of function and interaction rules. For example, the C/D snoRNA interaction predictor, PLEXY (Kehr et al. 2011), was developed to predict potential targets that interact with the canonical ASE sequence commonly used for rRNA modification. Indeed, PLEXY improves the efficiency of detecting canonical binding modes by only considering the 20 nucleotides upstream of the boxes D and D' of the snoRNA, corresponding to the ASE, and filters the interactions using previously identified pairing constraints (Chen et al. 2007). Accordingly, while PLEXY is efficient in identifying methylation targets, it has a limited use for identifying new forms of snoRNA-RNA interactions, especially those using an ASE independent homing sequence.

To uncover the full regulatory spectrum of box C/D snoRNAs and identify noncanonical interactions we developed snoGloBe, a C/D snoRNA interaction predictor based on a gradient boosting classifier. SnoGloBe considers all possible interactions between the snoRNA and targets regardless of the position within the snoRNA sequence. The predictor was trained and tested using known canonical interactions, experimentally detected large-scale snoRNA-RNA interactions datasets and validated noncanonical interactions from the human transcriptome. The accuracy and breadth of snoGloBe are evident from its capacity to recover most known snoRNA-RNA interactions, both canonical and noncanonical. Applying snoGloBe to the human coding transcriptome revealed positional enrichment of C/D snoRNA interactions in targets and functional enrichment for specific snoRNAs. The depletion of a model snoRNA altered the RNA level and splicing of a subset of the predicted targets. Notably, snoGloBe was also able to identify targets in a viral

genome including a known interaction in the SARS-CoV-2 transcriptome. Overall snoGloBe provides a flexible discovery tool for box C/D snoRNA interactions that transcends pre-established binding rules.

RESULTS

Identification and curation of experimentally identified snoRNA-RNA interactions

In order to create a predictor of snoRNA-RNA interactions, we began by extracting the canonical snoRNA interactions from snoRNABase (Lestrade and Weber 2006) and we combined it with experimentally validated noncanonical interactions reported in the literature. As a result, we identified 149 non-redundant interactions, 133 from snoRNABase and 16 from the literature (Figure 2A). In addition, we performed a de novo analysis of the datasets obtained from three high-throughput RNA-RNA interaction (HTRRI) identification methodologies PARIS (Lu et al. 2016), LIGR-seq (Sharma et al. 2016) and SPLASH (Aw et al. 2016) to extract new experimentally detected interactions. All sets were analyzed using the PARIS bioinformatics protocol (Lu et al. 2018) and filtered to remove interactions shorter than 13 base pairs and interactions featuring bulges (Figures 2B, S1). Overall, we identified 594 interactions listed in Table S1. The identified target biotypes varied greatly based on the data source underscoring the effect of the experimental approach and RNA source (Figure 2A). While snoRNABase is the main repository of canonical human snoRNA interactions, our manual curation of the literature revealed articles describing noncanonical snoRNA interactions and thus mainly involves protein coding targets. In contrast, PARIS, LIGR-seq and SPLASH are methodologies detecting RNA-RNA interactions with less experimenter bias. The widest distribution of target biotypes was identified in the HTRRI dataset and the largest number of distinct targets was found in protein coding RNAs (Figure 2A). The newly generated combined interaction set includes a wide variety of biotypes and interaction modes and forms an

excellent base for a positive set. To create a negative dataset, we generated a combination of random negative and matched negative interactions (Figure 2C). The random negative examples are random sequence pairs from any box C/D snoRNA and any gene, whereas the matched negative examples are random sequences originating from a snoRNA-target gene combination from the positive set (Figure 2D). The positive:negative ratio was chosen to be imbalanced (1:20) to reflect the fact that the proportion of transcriptomic sequences bound by C/D snoRNAs is expected to be much lower than the proportion not bound.

Feature encoding and predictor training

Since snoRNA-RNA interactions involve the formation of an RNA duplex, the sequences of the two RNAs must to be encoded amongst the features presented in input. The duplex length of validated canonical and noncanonical snoRNA interactions varies from 10 to 32 base pairs (Figure 2B, known canonical and known noncanonical), so we encoded the interaction sequences in windows of 13 nucleotides for both the snoRNA and its target. This compromise helps us take into account the validated snoRNA-RNA interactions while limiting the chance of finding these sequences randomly in the genome. The position of the interaction window in the snoRNA varies greatly between the canonical and noncanonical interactions. Indeed, canonical interactions employ only the regions immediately upstream of the boxes D or D' while the regions involved in noncanonical interactions cover the entire snoRNA length (Figure 1B). Therefore, we did not specify a fixed position but instead included it as an input feature. To gain information about the possible functional impact of the interactions we also included the target biotype as well as the position in the target (either in an exon and/or an intron and whether the exon is a 5' or 3' UTR when appropriate) as input features (Figure 2E). These input features were encoded for all positive and negative snoRNA-RNA pairs. Since snoRNA-RNA duplexes

are encoded as 13 nucleotide pairs of windows, an interaction can consist of multiple such pairs of windows. The resulting datasets consist of 1838 positive and 38370 negative windows (Figure 2C). The datasets were split in a non-overlapping manner for hyperparameter tuning, model training and model testing in a 1:7:2 relative proportion (Figure 2F). However, since there are few examples of known noncanonical interactions, they were all kept for the test set (Table S1). To avoid the redundancy caused by multicopy snoRNA genes (Bergeron et al. 2021; Deschamps-Francoeur et al. 2020) we made sure that members of the same snoRNA family (as defined by Rfam (Griffiths-Jones et al. 2003)) are present in only one dataset. For example, no member of the SNORD116 family is included in the test set if other members of the family are present in the training set (details in Methods section). Together the selection criteria allow the identification of a broad range of targets, reduce redundancy and decrease the dependency on the canonical mode of interaction.

SnoGloBe accurately predicts a wide range of interactions

The model used by snoGloBe is a gradient boosting classifier, which is a combination of multiple decision trees. The hyperparameters were tuned on 10% of the data, using a random search. The model was then trained on 70% of the data using a 5-fold stratified cross-validation (Figure 2E). The output of the prediction is a value between 0 and 1 representing the probability of interaction. The performance of the model was then evaluated on the test set and compared to both snoRNA specific and general predictors including PLEXY (Kehr et al. 2011), RNAup (Lorenz et al. 2011), RNAplex (Lorenz et al. 2011), RIsearch2 (Alkan et al. 2017) and IntaRNA (Mann et al. 2017) using the parameter values summarized in Figure S2. As indicated in Figure S3, snoGloBe clearly separated the negative and positive examples in the independent test set, giving the great majority of the negatives (96%) a score below 0.1 and the majority of positives (63%) a score

above 0.9. Notably, snoGloBe outperformed the other tools in predicting the snoRNA interactions by obtaining the highest area under the ROC and precision-recall curves (Figure 3A, B). PLEXY has the weakest performance, which is expected since it only predicts interactions with the ASE and the test set has interactions with all regions of the snoRNA (Figure S4). Interestingly, snoGloBe performs better than general RNA-RNA interaction predictors, hinting that snoGloBe is doing more than simple base-pair matching by capturing the specific information defining snoRNA - target interactions. By using thresholds to obtain a 90% precision with every tool, we determined the number of windows predicted as positive and negative for each tool (Figure S2). SnoGloBe retrieves the highest number of true positive windows, and the highest proportion of known canonical, known noncanonical interactions and HTRRI (Figures 3C, D, S5). PLEXY retrieves the smallest number of positive windows and most are from known canonical interactions. On the other hand, generic RNA-RNA interaction predictors give similar results amongst themselves and retrieve in majority known canonical interactions. Interestingly, although snoGloBe was not trained on any known noncanonical interaction, it outperformed the other tools by identifying 81/95 noncanonical windows (Figure 3D). Taken together, these data show that snoGloBe outperforms current predictors as it predicts more interactions with higher diversity and greater overall accuracy.

Transcriptome-wide snoGloBe predictions reveal an enrichment of snoRNA interactions in messenger RNA regulatory sequences

The interactions of every expressed human snoRNA were predicted against all protein coding genes in human. As many snoRNA copies in human are not expressed and likely represent ‘dead’ copies in the genome (Bergeron et al. 2021), we restricted our study to only those detected as expressed as described in the Methods section. To limit the number of predicted interactions, we used a stringent cut-off of 3 consecutive windows having a

probability (i.e. snoGloBe output score) greater than or equal to 0.98 (Figure S6). With this threshold, we obtain a median of 1017 predicted interactions per snoRNA (Figure 4A). SnoRNAs with the highest number of predicted interactions include snoRNAs with known validated targets like SNORD32A (>1500 interactions), SNORD83B (>6000 interactions) and SNORD88C (>10 000 interactions) (Elliott et al. 2019; Sharma et al. 2016; Scott et al. 2012). The global analysis of all snoRNA predicted interactions reveals a preference for the region upstream of the box D, even though interactions were predicted throughout the whole snoRNA length and the training and test sets displayed enriched interactions upstream of both the boxes D and D' (Figure 4B, Figure S4). Interestingly however, individual snoRNAs show different accumulation profiles along their length including some with a clear preference for targets binding the region upstream of the boxes D' or D and others with a square accumulation in regions other than those upstream of boxes D/D'. For example, SNORD45C displays two strong regions of target binding, found respectively upstream of the boxes D' and D (Figure S7A). On the other hand, SNORD11 has only one such region, upstream of the box D (Figure S7B). In contrast, SNORD31B in Figure S7 panel C and SNORD18A in panel D both have only one clear target binding region, overlapping and downstream of the box D'. Interestingly, while most snoRNA target sequences were located in introns, we detected enrichment in the exons and exon-intron junctions when compared to the distribution of these features in the transcriptome (Fig 4 compare panels C and D). Indeed, the protein coding transcriptome consists of 7.26% exonic sequences and 0.03% intron-exon junctions (measured in terms of 13 nt windows as described above), while 15.65% and 1.19% of the predicted snoRNA interactions are found in these regions respectively, representing increases of >2 folds in exonic sequences and 40 folds in intron-exon junctions. Many exonic snoRNA interactions are found in the 5' or 3' UTRs (Figure 4E, F), suggesting a role in regulating translation, transcript stability and/or 3' end processing. Binding of snoRNAs to exonic sequence

accumulates in precise regions or hot spots arguing for an organized binding program (Figure 4G). We conclude that binding of snoRNAs is not randomly distributed in the human transcriptome but targets specific regulatory elements and in particular those regulating splicing and translation.

SnoGloBe uncovers functional specialization of snoRNA

Surprisingly, we found that snoRNAs do not feature uniform binding patterns or target preferences but instead display snoRNA or snoRNA family specific binding patterns. For example, while SNORD35A prefers to bind to the 3' splice site, snoU2-30 binding is enriched in the 5' splice sites while SNORD38A shows an enrichment on the polypyrimidine tract (PPT) (Figure S8). Some snoRNAs display even more convincing target sets, including strong enrichment in specific gene elements of target genes enriched in specific biological processes, as well as significant overlap with functionally relevant RNA binding protein (RBP) target sites. For example, SNORD50B was found to be strongly enriched in 5'UTR binding of its targets and using its box D adjacent guide region (Figure S9A, B). Gene ontology enrichment analyses show that predicted targets of SNORD50B are involved in neuronal functionality and genes coding for proteins related to cell-cell interactions (Figure S9C). Many SNORD50B exonic targets bind alternative 5'UTRs, involving alternative transcription start sites, such as those of NDFIP2, COPS3 and SPG21, which could lead to transcript-specific effects (Figure S10). These possible regulatory events of SNORD50B are not randomly distributed but appear to target specific group of genes. In contrast to SNORD50B which is specialized in targeting alternative 5' UTRs, SNORD22 shows enriched binding at the 3' splice sites and PPTs of its targets, involving a non-ASE region of the snoRNA overlapping with the box C' (Figure S11A, B). Many SNORD22 3' splice site targets bind alternatively spliced exons including in the diacylglycerol kinase zeta gene DGKZ, the amyloid beta precursor protein binding family

B member APBB1 and three hits on the same alternatively spliced exon in the focal adhesion protein PXN (Figure S12). Gene ontology terms for SNORD22 targets are enriched in membrane proteins, cell junctions and GTPases (Figure S11C). Together these data indicate that snoRNAs use different mechanisms to identify their targets, co-regulating players of a common cellular function.

Overlap of the binding sites of snoRNAs and RNA binding proteins

Comparison between the snoRNA binding sites identified by snoGloBe and the binding sites of RNA binding proteins (RBP) as determined by the ENCODE project using eCLIPs (Van Nostrand et al. 2020; Davis et al. 2018) indicated strong overlap between the two. For example, both SNORD50B and SNORD22, which show strong position enrichment and functional enrichment of their targets, show strong overlap of their binding sites with those of specific RBPs (Figure S9D, S11D). In the case of SNORD50B, the strongest enrichments include DDX3X a helicase known amongst others to bind RNA G-quadruplexes in 5'UTRs, NCBP2 a cap-binding protein interacting with pre-mRNA, BUD13 involved in pre-mRNA splicing and FTO an RNA-demethylase involved in the maturation of mRNAs, tRNAs and snRNAs, supporting a role for SNORD50B in the maturation of pre-mRNA and in particular their 5' extremity. In contrast, for SNORD22, the RBPs with strongest enrichment are PCBP2 the poly(rC) binding protein, PTBP1 a PPT binding protein involved in the regulation of alternative splicing as well as BUD13, PRPF8 and AQR all known as involved in pre-mRNA splicing, supporting a role for SNORD22 in the regulation of alternative splicing, through the binding of PPTs. These data suggest that snoRNAs may influence RBP function through collaborative or competitive binding to the targeted RNA sequence.

SnoGloBe predicts functional regulatory targets

To evaluate the functional significance of snoGloBe's predicted interactions, we experimentally measured the impact of knocking down a model snoRNA on its predicted targets. We chose SNORD126 as a model since it was implicated in different cellular functions while most of the targets relevant to these functions remain unidentified. This snoRNA was originally thought to be an orphan (Lestrade and Weber 2006), but was later predicted to interact with and then shown to conditionally methylate the 28S rRNA (Jorjani et al. 2016; Hebras et al. 2019). In addition, it was shown that SNORD126 can activate the PI3K-AKT pathway through a yet to be determined mechanism (Fang et al. 2017). The SNORD126 interactions predicted by snoGloBe against protein coding genes led to interesting profiles. Most of the snoGloBe predicted interactions for this snoRNA involve a non ASE sequence overlapping the D' box suggesting noncanonical methylation independent functions (Figure 5A and B). SNORD126 interactions are enriched in exons (1.6 fold) and particularly enriched on intron-exon junctions (>50 fold) compared to the protein coding transcriptome composition (Figure 5C-D). The exons predicted to be targeted by SNORD126 are enriched in 5'UTR (Figure 5E-F). SNORD126 predicted interactions are mostly uniformly distributed in the target exons, with the exception of notable enrichment around 80 nucleotides upstream of the exons (Figure 5G). These data suggest that SNORD126 may regulate gene expression through modulation of RNA stability and/or splicing.

To evaluate the impact of SNORD126 on splicing and RNA stability we knocked it down using RNase H dependent antisense oligonucleotides and monitored the impact on the transcriptome using RNA-seq. The knockdown was performed in the HepG2 cell line, which is frequently used in genome wide analysis (Davis et al. 2018). In this cell line, 798 predicted target genes are expressed at 1 TPM or higher. Overall, the knockdown of SNORD126 resulted in the up regulation of 340 genes and the down regulation of 710

genes, totalling 1050 protein coding genes, 65 of which are snoGloBe's predicted targets (Fig. 5H). The overlap between the predicted targets and the differentially expressed genes shows a significant enrichment (p-value < 0.0001 by random sampling analysis as described in the Methods). The most upregulated predicted target following SNORD126 knockdown is BNIP3L, a pro-apoptotic protein, and the predicted interaction is located in the intron. The upregulation of BNIP3L following SNORD126 knockdown is in line with SNORD126 oncogenic role through the activation of PI3K-AKT pathway (Fang et al. 2017) and this predicted interaction could be an interesting lead to elucidate the underlying mechanism. On the other hand, the most downregulated predicted target is DNAH17, a dynein component, and has two predicted binding sites, one in an exon and one in an intron, around 300 nucleotides upstream the exon. These data suggest that one snoRNA can have different effect depending on the binding characteristics, such as the number of interactions and their region.

In addition to the change in expression, SNORD126 knockdown also altered the alternative splicing of transcripts. 309 such events are affected by the knockdown of SNORD126, 9 of which overlap a predicted SNORD126 binding site (p-value = 0.002). Amongst the interesting candidates, the target site of SNORD126 on CPT1B, encoding a carnitine O-palmoyltransferase, overlaps an alternative 5' splice site detected with a differential splicing pattern and the target site of SNORD126 on MR1, which encodes a hydrolase involved in the NF-kB pathway, is near a 3' splice site for which the intron has an alternative 5' extremity (Figure S13). Interestingly, three genes having an alternative splicing event overlapping a predicted interaction were also differentially expressed upon SNORD126 knockdown: CPT1B, MR1 and DDX11, hinting that SNORD126 could affect RNA stability through alternative splicing.

To further evaluate snoGloBe's performance in predicting functionally relevant interactions, we compared it to PLEXY (Kehr et al. 2011) and RIsearch2 (Alkan et al. 2017), the general RNA-RNA interaction predictor with the best area under the ROC and Precision-Recall curves on the test set (Figure 3A, B). We used an energy threshold of -20.4 kcal/mol, which is the average of snoRNA-rRNA duplexes recovered by PLEXY (Kehr et al. 2011). Comparing the predicted interactions obtained by each tool in the protein coding transcriptome to SNORD126 knockdown shows that snoGloBe retrieves a greater number of interactions in differentially expressed genes and alternative splicing events upon SNORD126 knockdown with fewer predicted interactions than the other tools, leading to a lower number of false positives (Figure 5I). PLEXY performs similarly to snoGloBe on the prediction of differential expression targets, but the overlap between snoGloBe and PLEXY predicted targets is small, hinting that both tools use different information and complement each other (Figure S14). RIsearch2 has the highest number of false positives, underlining the importance of using snoRNA specific predictor to delineate high confidence interactions. Even though snoGloBe provides an enhancement in the prediction of functional targets compared to other tools, not all predicted targets are affected by SNORD126 knockdown and several non-predicted targets were affected reflecting the complexity of the biological system that could vary depending on the cell line, growth conditions and propensity to secondary effects. The power of snoGloBe in predicting functionally relevant targets is evident when compared to HTTRI. In contrast to snoGloBe predictions of SNORD126 for which a total of 72 were detected as either stability and/or splicing targets following SNORD126 knockdown, only two SNORD126 interactions were identified in the HTRRI datasets, neither of which is detected as affected by the SNORD126 knockdown, emphasizing the usefulness of snoGloBe in addition to high-throughput methodologies. We conclude that snoGloBe is an efficient tool for the prediction of biologically relevant snoRNA-RNA interactions.

SnoGloBe predicts interactions between human snoRNAs and the SARS-CoV-2 transcriptome

As another example of the utility of snoGloBe, we applied it to the SARS-CoV-2 transcriptome. It has been shown that the SARS-CoV-2 genome is heavily 2'-O-ribose methylated and interacts strongly with snoRNAs using the high-throughput structure probing methodology SPLASH (Aw et al. 2016; Yang et al. 2021). Thus as another proof of concept for the utility and capacity of snoGloBe, we predicted the interactions between human snoRNAs and the SARS-CoV-2 genome using snoGloBe. We detected 8818 interactions between 312 snoRNAs and the SARS-CoV-2 genome, the distribution of which is shown in Figure 6A. One of the strongest interaction partners between SARS-CoV-2 and host transcripts detected experimentally using SPLASH is with the box C/D snoRNA SNORD27 (Yang et al. 2021). Although, the SPLASH experiments were carried out in Vero-E6 cells from African green monkey kidney, snoGloBe detects the SARS-CoV-2 interaction with human SNORD27 (Figure 6B), suggesting that the interaction is also relevant in human.

SnoGloBe availability and usage

The snoGloBe code is written in Python using the machine learning package scikit-learn (Pedregosa et al. 2011). It is freely available and can be downloaded from gitlabscottgroup.med.usherbrooke.ca/scott-group/snoglobe. Users must provide a file with the sequences of the snoRNAs of interest, the sequences of whole chromosomes, an annotation file in gtf format and a file with the potential target identifiers to scan for snoRNA interactions. Detailed instructions are available in the help manual.

DISCUSSION

Motivated by the continually increasing number of examples of snoRNAs interacting with noncanonical targets using diverse regions within but also without the ASE (Figure 1) as well as by the diversity in RNAs targeted by snoRNAs (Figure 2A), we built snoGloBe, a box C/D snoRNA interaction predictor that considers the whole snoRNA and any type of RNA target. SnoGloBe is a gradient boosting classifier that takes into account the sequence of the snoRNA and its potential target as well as the position in the snoRNA and the type and position in the potential target. Compared to general use RNA-RNA interaction predictors that consider only sequence complementarity and the interaction stability of the duplex, snoGloBe performs considerably better, suggesting that considering snoRNA and target features enhances the prediction. SnoGloBe also performs better than the snoRNA-specific predictor PLEXY which was not built to predict interactions outside of the snoRNA ASEs. Many such non-ASE interactions are detected in HTRRI datasets and some have been extensively validated for individual snoRNAs (Figure 1B), limiting the scope of the PLEXY predictor. Interestingly a subset of positive examples (30%) is not found by snoGloBe and while this proportion is considerably lower than for all other predictors considered (they miss >70% of positives in the test set, Figure 3D), there is still room for improvement. This subset involves mostly interactions displaying bulges in the base pairing in one or both members of the interaction, which are more difficult to accurately identify and will require different approaches and likely larger training datasets for machine learning approaches to accurately predict them.

The study of the snoGloBe predicted interactions in human is very interesting and opens numerous research avenues that will likely lead to important insights into snoRNA function. Dozens of snoRNAs display profiles supporting the non-uniform distribution of predicted targets in pre-mRNA, with hundreds or even thousands of targets enriched in common regulatory elements such as PPTs, 5’ or 3’ splice sites and 5’ or 3’ UTRs (Figures

4, 5, S8, S9, S11). Each such snoRNA target profile will require in depth integrative analysis to consider the possible functionality, molecular mechanism and ultimately cellular outcome of the collective regulation of these targets by the snoRNA. We began such studies for SNORD50B, SNORD22 and SNORD126, all three of which display strong enrichment for binding to specific regulatory elements, respectively 5' UTRs, PPTs/3' splice sites and 3' of introns. Manual review of their predicted targets led to the identification of a subset of such binding events overlapping alternatively regulated events (for example alternative 5' UTRs for SNORD50B and alternatively spliced exons for SNORD22, Figures S10, S12). Gene ontology analysis of the targets show strong enrichment for specific biological processes and provide convincing subsets of targets to focus on. Finally the strong overlap between snoRNA predicted binding sites and ENCODE-detected RBP binding sites is important evidence of the functional relevance of the interactions, particularly as the function of the RBPs with the strongest overlap strongly supports the type of regulation likely carried out by the snoRNA. Several molecular mechanisms could explain the binding overlap of snoRNA and RBP at the same position on the same target pre-mRNA. The snoRNA could be guiding the RBP to its target as snoRNAs do for core snoRNA binding proteins such as FBL, and as has been reported for nuclear exosome components as shown in (Zhong et al. 2015). However, since RNA binding motifs are known for several of the RBPs considered and because snoRNAs have not been found as enriched binding partners of all these RBPs, it is likely that the snoRNAs and some of the RBPs are competing for the same binding site. Further studies will be required to define the snoRNA-RBP relationship and its effect on the regulation of the targets. These overlapping snoRNA-RBP targets could be revealing novel levels of post-transcriptional regulation, the understanding of which will be important in health and disease.

Analysis of the newly predicted targets suggests that snoRNAs play an important role in regulating the splicing and stability of protein coding RNA. Indeed, the knockdown of a model snoRNA altered the stability and splicing of predicted targets even when tested in a single cell line and growth condition. Comparison with other tools showed that snoGloBe is able to retrieve a higher number of functional targets with fewer predictions, followed by PLEXY (Figure 5I). The low overlap between the differentially expressed targets predicted by both tools indicates that they can be used together to identify more valid targets (Figure S14). SnoRNA-RNA interactions are short, which is reflected in their minimal free energy. Hence, when using general RNA-RNA interaction predictors, the minimal free energy threshold can't be set to a very stringent value, resulting in a vast number of reported interactions, emphasizing the importance of snoRNA specific tools to help narrow the search and rapidly identify high confidence candidates. Meanwhile, by considering the ensemble of the data generated by snoGloBe, certain missed targets could be identified by virtue of independent neighbourhood analysis or similarity of their effects on cellular phenotype. Clearly most targets need to be ultimately validated experimentally and datasets like HTRRI will remain valuable resources. However, the limitation of most experimental approaches including the consideration of too few cell types and growth conditions as well as the cost and time involved makes them less useful for uncovering new targets and condition-specific binding events.

Overall, while HTRRI datasets have collectively been generated in a handful of cell lines, considerable time and money would be required to explore normal human tissues and diverse conditions using these methodologies. SnoGloBe predictions will be instrumental in filling the gap by providing rapid predictions for snoRNA interactions that can then be further investigated to better understand cellular functionality. Our additional

demonstration that snoGloBe can be used to investigate the interactions between snoRNAs and viral transcripts (Figure 6), further widens its scope and utility.

METHODS

High-throughput RNA-RNA interaction analysis

The high-throughput RNA-RNA interaction datasets from PARIS (Lu et al. 2016) (SRR2814761, SRR2814762, SRR2814763, SRR2814764 and SRR2814765), LIGR-seq (Sharma et al. 2016) (SRR3361013 and SRR3361017) and SPLASH (Aw et al. 2016) (SRR3404924, SRR3404925, SRR3404936 and SRR3404937) were obtained from the short read archive SRA (Leinonen et al. 2011) using fastq-dump from the SRA toolkit (v2.8.2). The PARIS datasets were trimmed using the icSHAPE pipeline available at https://github.com/qczhang/icSHAPE. PCR duplicates were removed from LIGR-seq datasets using the script readCollapse.pl from the icSHAPE pipeline and the reads were trimmed using Trimmomatic version 0.35 with the following options : HEADCROP:5 ILLUMINACLIP:TruSeq3-SE.fa:2:30:4 TRAILING:20 MINLEN:25 (Bolger et al. 2014). The quality of the reads was assessed using FastQC (v0.11.15) before and after the pre-processing steps (Andrews 2010). All the samples were analyzed using the PARIS pipeline as described in sections 3.7 and 3.8 from (Lu et al. 2018). Some modifications were made to the duplex identification and annotation scripts. The modified scripts are available at gitlabscottgroup.med.usherbrooke.ca/gabrielle/paris_pipeline.

The RNA duplexes were assigned to genes using the annotation file described in (Boivin et al. 2018) to which missing rRNA annotations from RefSeq (O'Leary et al. 2016) were added. The annotation file was modified using CoCo correct_annotation (Deschamps-Francoeur et al. 2019) to ensure the correct identification of snoRNA interactions.

Only the interactions between two known genes including a box C/D snoRNA were kept. To avoid intramolecular interactions, we removed interactions between a snoRNA and its

50 flanking nucleotides and interactions between two snoRNAs of a same Rfam family (Griffiths-Jones et al. 2003). To limit the number of false positives, we filtered the interactions based on their pairing using RNAplex (Lorenz et al. 2011). Only paired regions of the interactions were kept to get rid of unpaired flanking regions. The interactions were split at each bulge to ensure the correct alignment of the snoRNA and target sequences. The interactions shorter than 13 nucleotides were removed to respect the length of the windows (see Input features section). We finally removed interactions that were already known and present in our positive set described in the next section. We obtained 445 box C/D snoRNA interactions (Figure S1).

Positive set composition

The positive set is composed of the previously detected snoRNA interactions from PARIS, LIGR-seq and SPLASH filtered as described above, as well as interactions obtained from snoRNABase (Lestrade and Weber 2006) and manually curated interactions from the literature (Table S1) (Figure 2A, B). Interactions from snoRNABase and from the literature that were shorter than 13 nucleotides were padded by adding their flanking sequence to respect the length threshold.

Negative set composition

The negative set is composed of random negatives and matched negatives (Figure 2C). The random negative examples are the combination of random sequences from any box C/D snoRNA and any gene, whereas the matched negative examples are random sequences coming from a positive snoRNA-target gene combination (Figure 2D).

Input features

The interactions were split in 13 nucleotide sliding windows, with a step of 1 nucleotide. The 13 nucleotide window length was chosen to limit the chance of finding this sequence randomly in the genome, and most of the known interactions respect this length (Figure 2B). Each interaction window is composed of 13 nucleotides of the snoRNA and the corresponding 13 nucleotides of the target. The input features used are the window sequences in one-hot encoding, the relative position in the snoRNA between 0 and 1, the location in the target gene (intron, exon, 3'UTR and/or 5'UTR) and the target biotype (Figure 2E). The biotypes considered are listed in snoGloBe's manual. Protein coding, pseudogene and long noncoding RNA biotypes were grouped according to http://vega.archive.ensembl.org/info/about/gene_and_transcript_types.html and http://ensembl.org/Help/Faq?id=468.

Redundancy removal for tuning, training and test sets

The positive and negative examples were split into hyperparameter tuning, training and test sets. First, to remove redundancy from the sets, the snoRNAs were grouped based on their Rfam identifier (Griffiths-Jones et al. 2003). To ensure that the model is not trained and tested on similar snoRNAs, the Rfam families were split in order to assign 20% of all examples in the test sets, with similar proportion of the initial HTRRI and known canonical interactions. All the known noncanonical interactions were kept for the test sets since there are very few such examples. The remaining examples were split between the hyperparameter tuning and training sets to consist respectively of 10% and 70% of initial data (Figure 2F).

Building the model

The model used is a gradient boosting classifier from scikit-learn (v0.21.3) (Pedregosa et al. 2011). We selected the hyperparameters using a random search with 3-fold cross-validation. The selected hyperparameters are: n_estimators = 371, min_samples_split = 76, min_samples_leaf = 49, max_depth = 2 and learning_rate = 0.43, others are kept to default.

The model was trained on the whole training set and validated with 5-fold stratified cross-validation, to keep similar proportions of HTRRI and known canonical interactions in each subset. The resulting model is called snoGloBe.

The model performance was evaluated on the test set and compared to PLEXY (Kehr et al. 2011), RNAplex (Lorenz et al. 2011), RIsearch2 (Alkan et al. 2017), IntaRNA (Mann et al. 2017) and RNAup (Lorenz et al. 2011). To compare their performance on a similar basis, we selected a threshold (either a score for snoGloBe, or an energetic cut-off for the other tools) resulting in 90% precision on the test set. The details are available in Figure S2. PLEXY was only used for snoRNAs with non-degenerated boxes D and D' to avoid bias caused by misidentified boxes.

Prediction against protein coding genes

SnoGloBe was used to predict box C/D snoRNA interactions with protein coding transcripts. For this analysis, only box C/D snoRNAs expressed at 1 transcript per million (TPM) or more in at least one of the RNA-seq datasets from 7 different healthy human tissues (3 samples from different individuals for each of the following tissues: brain, breast, liver, ovary, prostate, skeletal muscle and testis) from a previous study (Fafard-Couture et al. 2021) (available from GEO: GSE126797, GSE157846) were considered, totaling 312 snoRNAs. We predicted the interactions of these snoRNAs against all protein coding genes, split in 13-nucleotide windows with a step of two. We took whole gene sequences to predict interactions with any intron and exon. To narrow the number of predictions

obtained, we kept the interactions having at least three consecutive windows with a score >= 0.98 for further analysis. The gene ontology enrichment analysis of the predicted targets was done using g:Profiler (Raudvere et al. 2019).

Overlap between predicted snoRNA interactions and eCLIP region

All the eCLIP datasets (Van Nostrand et al. 2020, 2016) were downloaded from the ENCODE portal (Davis et al. 2018), totaling 225 samples considering 150 proteins. The complete list of the datasets is available in Table S2. Only the eCLIP regions having a p-value <= 0.01 were kept. Datasets from the same protein were merged using BEDTools merge -s (v2.26.0) (Quinlan and Hall 2010). The number of overlaps between the predicted interactions and the eCLIP regions was computed using BEDTools intersect -s.

SNORD126 knockdown

HepG2 cells were cultured in complete Eagle's Minimum Essential Medium (EMEM from Wisent) and passaged twice a week, according to ATCC guidelines. Trypsinized cells were then seeded at 350000 cells/well in 6 well plates in 1ml EMEM. Cells were transfected 24 hours later with 2 different ASOs targeting SNORD126 (30nM or 40nM) using Lipofectamine 2000 (LIFE technologies) and optiMEM (Wisent). A scrambled ASO was used as a negative control. The sequence of the ASOs are listed in Supplemental Figure S15.

Cells were harvested 48 hours post transfection, washed and pelleted, then resuspended in 1ml Trizol and stored at -80℃ until RNA extraction. This was repeated 3 times to obtain biological triplicates.

RNA extraction

Total RNA extraction from transfected HepG2 cells was performed using RNeasy mini kit (Qiagen) as recommended by the manufacturer including on-column DNase digestion with RNase-Free DNase Set (Qiagen). However, 1.5 volumes Ethanol 100% was used instead of the recommended 1 volume ethanol 70% in order to retain smaller RNA. RNA integrity of each sample was assessed with an Agilent 2100 Bioanalyzer. RNA was reversed transcribed using Transcriptor reverse transcriptase (Roche) and knockdown levels were evaluated by qPCR.

RNA-seq library preparation and sequencing

RNAseq libraries were generated from 1ug DNA-free total RNA/condition using the NEBNext® Ultra™ II Directional RNA Library Prep Kit for Illumina (E7760S) and following the Protocol for use with NEBNext Poly(A) mRNA Magnetic Isolation Module (NEB #E7490). The resulting libraries were submitted to a total of 10 cycles of amplification then purified using 0.9X Ampure XP beads. Quality and size was assessed with an Agilent 2100 Bioanalyser. Libraries were then quantified using a Qubit fluorometer, pooled at equimolar concentration and 1.8pM was sequenced on Illumina's NextSeq 500 using a NextSeq 500/550 High Output Kit v2.5 (150 cycles) paired-end 2x75bp.

RNA-seq analysis

The resulting base calls were converted to fastq files using bcl2fastq v2.20 (Illumina) with the following options: --minimum-trimmed-read-length 13, --mask-short-adapter-reads 13, --no-lane-splitting. The fastq files were trimmed for quality and to remove remaining adapters using Trimmomatic v0.36 (Bolger et al. 2014) with ILLUMINACLIP:{adapter_fasta}:2:12:10:8:true, TRAILING:30, LEADING:30, MINLEN:3. The sequence quality was assessed using FastQC v0.11.5 (Andrews 2010) before and after the trimming. The trimmed sequences were aligned to the human genome (hg38)

using STAR v2.6.1a (Dobin et al. 2013) with the options --outFilterScoreMinOverLread 0.3, --outFilterMatchNminOverLread 0.3, --outFilterMultimapNmax 100, --winAnchorMultimapNmax 10, --alignEndsProtrude 5 ConcordantPair. Only primary alignments were kept using samtools view -F 256 (v1.5) (Li et al. 2009). The gene quantification was done using CoCo correct_count -s 2 -p (v0.2.5p1) (Deschamps-Francoeur et al. 2019). DESeq2 was used for the differential expression analysis (Love et al. 2014). Genes having a corrected p-value <= 0.01 were considered significantly differentially expressed. The alternative splicing analysis was done using MAJIQ v2.2 and VOILA with the option --threshold 0.1 (Vaquero-Garcia et al. 2016).

Empirical p-value calculation

To evaluate the significance of the overlaps between each snoRNA predicted interaction and eCLIP binding sites, alternative splicing events and differentially expressed genes, we computed an empirical p-value using BEDTools shuffle 10 to 100 000 times for each combination followed by BEDTools intersect -s through pybedtools (Quinlan and Hall 2010; Dale et al. 2011). BEDTools shuffle was used with an appropriate background for each analysis: all protein coding genes for eCLIP binding sites and protein coding genes having an average of 1TPM across all sequencing datasets for differential expression and alternative splicing analyses. We counted the number of distinct events, or genes in the case of differential expression analysis, having an overlap with at least one shuffled interaction for each iteration. P-values were calculated as the proportion of iterations in which the shuffled dataset overlap was at least as extreme as the true dataset overlap.

Prediction of human snoRNA interaction with SARS-CoV-2 transcriptome

We predicted the interactions between the expressed human snoRNAs against SARS-CoV-2 transcriptome, using SARS-CoV-2 ASM985889v3 genome assembly and the

annotation file Sars_cov_2.ASM985889v3.101.gtf obtained from Ensembl COVID-19 (Howe et al. 2021). We used thresholds of a minimum of 3 consecutive windows having a probability greater or equal to 0.85.

COMPETING INTERESTS STATEMENT

The authors declare no competing interests.

ACKNOWLEDGEMENTS

The authors would like to thank members of the Scott and Abou-Elela groups for helpful discussions and Compute Canada for providing state-of-the-art computing infrastructures. This work was supported by a CIHR grant (PJT 153171) to MSS and SAE and a team FRQ-NT grant to MSS and SAE. GDF was supported by a NSERC Doctoral scholarship. MSS holds a Fonds de Recherche du Québec – Santé (FRQ-S) Research Scholar Senior Career Award. SAE and MSS are members of the Centre de Recherche du Centre Hospitalier de l'Université de Sherbrooke.

FIGURE LEGENDS

Figure 1. Box C/D snoRNA characteristics and interactions. A) Box C/D snoRNAs have well conserved patterns, called boxes C/C' (green) and D/D' (purple). The canonical interaction with the target (orange) occurs upstream of the boxes D and D', using a region referred to as the ASE. The fifth nucleotide upstream of these boxes is methylated by the core C/D snoRNA interactor FBL. B) Schematic representation of experimentally validated noncanonical interaction regions. The classical elements are represented: the boxes C and C' (green), D and D' (purple) and the ASE (yellow). Bipartite interactions are represented by a dotted line. The names of the interacting snoRNA and target gene are indicated on the right. The color of the interaction represents its effect, whether regulation of alternative splicing, regulation of RNA level (either pre-mRNA or mRNA) and RNA modification including methylation of noncanonical targets, acetylation and A to I editing. Combined together, noncanonical interactions cover the whole snoRNA. [a] (Falaleeva et al. 2016), [b] (Elliott et al. 2019), [c] (Zhong et al. 2015), [d] (Sharma et al. 2016), [e] (Scott et al. 2012), [f] (Kishore and Stamm 2006), [g] (Vitali et al. 2005), [h] (Patterson et al. 2017), [i] (Bachellerie et al. 1995), [j] (Sharma et al. 2017)

Figure 2. Composition of the dataset used to build snoGloBe. A) Diverse RNAs have been shown to bind box C/D snoRNAs. Interactions involving box C/D snoRNAs were collected and assembled including known canonical interactions with rRNA and snRNA from snoRNABase, known noncanonical interactions curated from the literature and interactions extracted from HTRRI datasets. The proportion of interactions involving different RNAs of each biotype is shown for each interaction source. The color legend for RNA biotypes is shown on the right. (B) Distribution of the length of interactions from each data source. (C) Distribution of the datasets used to build snoGloBe. The dataset consists of positive, matched negatives and random negatives in a proportion of 20 negatives for

1 positive window. The positive windows are composed of HTRRI (86.3 %), known canonical (8.5 %) and noncanonical (5.2 %) interactions. (D) Generation of matched negative windows. 10 matched negative windows are generated for each positive one. The matched negative windows originate from the same snoRNA–target gene pair as the positive window. One has the same position in the snoRNA and a different position in the same target, one has a different position in the snoRNA and the same position in the target, and 8 windows have random positions in the same snoRNA-target pair. E) SnoRNA-RNA pairs are encoded for presentation to the predictor. Features considered include the 13 nucleotide sequence of the snoRNA and the 13 nucleotide sequence of the target, the relative position of the window in the snoRNA, the target biotype and the position in the target. F) The dataset is split in non-overlapping sets for hyperparameter tuning (10% of the windows), training (70% of the windows) and testing (20% of the windows). The hyperparameter tuning was done using a random search with 3-fold cross-validation. The model was trained and evaluated using stratified 5-fold cross-validation to ensure the correct representation of each category of positive windows in each subset. The known noncanonical windows were all kept for the validation set.

Figure 3. SnoGloBe performs better than available tools. (A) Receiver Operator Characteristic (ROC) and (B) Precision-Recall (PR) curves of different tools calculated on the test set. The corresponding area under the curves (AUC) are indicated in the legend. C) Table of performance measures from different tools calculated on the test set with a threshold set to obtain a precision of 90%. PLEXY was only used on interactions from box C/D snoRNA with non-degenerated boxes D and D' (Table S1) since the position and sequence of the boxes are required. D) Upset plot representing the overlaps between each tool prediction of the test set's positive windows. The upset plot only shows the

subset of the interactions that were considered for PLEXY to ensure a fair comparison. The upset plot of all the test set's positive windows is shown in Figure S5.

Figure 4. Box C/D snoRNA predicted interactions across the coding transcriptome. A) Histogram and boxplot (above) of the number of interactions per snoRNA using a threshold of at least 3 consecutive windows having a probability greater or equal to 0.98. Most snoRNAs have less than 2000 predicted interactions. B) Distribution of the predicted region of interaction in all snoRNAs. The position in the snoRNAs is normalized between 0 and 1. The computationally identified boxes C, D' and D are respectively represented in green and purple. The predicted interactions are found throughout the snoRNA, with an enrichment in the 3' end. C-D) Bar chart representing the proportion of exon, intron and intron-exon junction in the protein coding transcriptome (C) and the box C/D predicted interactions in the targets (D). The predicted interactions are enriched in the exons and the intron-exon junctions (D) compared to the protein coding transcriptome (C). E-F) Doughnut charts representing the composition in terms of 13-nt windows of the exons of the protein coding transcriptome (E) and the box C/D snoRNA predicted interactions in the targets (F). The predicted interactions located in exons are mainly found in UTRs (F) and are enriched in 5'UTRs when compared to the protein coding transcriptome (E). G) Distribution of the predicted interactions 100 nucleotides upstream of exons (left), in the exon (middle), and 100 nucleotides downstream of the exons (right). The positions in the exons are normalized between 0 and 1. The number of interactions is normalized by the number of existing features (exons or introns) at each position multiplied by one million. The predicted interactions are uniformly distributed across the exons, there is a higher number of interactions predicted inside the exons than in the flanking nucleotides.

Figure 5. SNORD126 predicted targets are significantly affected by its knockdown. A) The major interaction site in SNORD126 predicted by snoGloBe is located in the middle

of the snoRNA and doesn't match the ASE upstream of the boxes D and D' represented in purple. The accumulation profile represents the proportion of SNORD126 predicted interactions overlapping each nucleotide in the snoRNA (blue) and the interactions predicted in differentially expressed (DE) genes (orange). B) Predicted folded structure of SNORD126 considering the main region of interaction. Mfold (Zuker 2003) was used to predict the secondary structure of SNORD126, forcing nucleotides 37 to 53 to be single stranded (blue) through the unafold webserver. C-D) SNORD126 predicted interactions are enriched in the exons and the intron-exon junctions. (C) Shows the relative length of the different elements of the protein coding transcriptome while (D) shows the relative proportion of the targets of SNORD126. E-F) The predicted interactions located in exons are enriched in 5'UTRs. (E) Doughnut chart showing the breakdown of the different constituents of exons in the protein coding transcriptome. (F) Doughnut chart showing the same breakdown but only for regions targeted by SNORD126. G) SNORD126 predicted interactions are uniformly distributed across exons, with an enrichment around 80 nucleotides upstream of exons. H) Volcano plot representing the impact of SNORD126 knockdown on protein coding genes. The dots above the gray line are considered significantly differentially expressed (adjusted p-value ≤ 0.01). SNORD126 predicted targets are colored in blue. Only genes having a mean of 1 TPM across all samples are shown. (I) Bar plot representing the number of experimentally validated events (LSV : local splicing variation, DEG: differentially expressed gene) having at least one overlapping predicted interaction per thousand total SNORD126 predicted interactions by snoGloBe, PLEXY and RIsearch2.

Figure 6. Human box C/D snoRNAs are predicted to target the SARS-CoV-2 transcriptome. A) Distribution of the number of predicted interactions per snoRNA across the SARS-CoV-2 transcriptome. Human box C/D snoRNAs have a median of 22 predicted

interactions having at least 3 consecutive windows with a score greater or equal to 0.85 with SARS-CoV-2 transcriptome. B) The validated interaction between African green monkey SNORD27 and SARS-CoV-2 is also predicted with human SNORD27. The validated interaction is shown in red, the nucleotide that differs between the African green monkey and human SNORD27 is underlined. The predicted interaction is outlined by the box.

REFERENCES

Alkan F, Wenzel A, Palasca O, Kerpedjiev P, Rudebeck AF, Stadler PF, Hofacker IL, Gorodkin J. 2017. RIsearch2: suffix array-based large-scale prediction of RNA-RNA interactions and siRNA off-targets. *Nucleic Acids Res* **45**: e60.

Andrews S. 2010. FastQC: A Quality Control tool for High Throughput Sequence Data. https://www.bioinformatics.babraham.ac.uk/projects/fastqc/ (Accessed July 5, 2021).

Aw JGA, Shen Y, Wilm A, Sun M, Lim XN, Boon K-L, Tapsin S, Chan Y-S, Tan C-P, Sim AYL, et al. 2016. In Vivo Mapping of Eukaryotic RNA Interactomes Reveals Principles of Higher-Order Organization and Regulation. *Mol Cell* **62**: 603–617.

Bachellerie JP, Nicoloso M, Qu LH, Michot B, Caizergues-Ferrer M, Cavaille J, Renalier MH. 1995. Novel intron-encoded small nucleolar RNAs with long sequence complementarities to mature rRNAs involved in ribosome biogenesis. *Biochem Cell Biol Biochim Biol Cell* **73**: 835–843.

Bergeron D, Laforest C, Carpentier S, Calvé A, Fafard-Couture É, Deschamps-Francoeur G, Scott MS. 2021. SnoRNA copy regulation affects family size, genomic location and family abundance levels. *BMC Genomics* **22**: 414.

Boivin V, Deschamps-Francoeur G, Couture S, Nottingham RM, Bouchard-Bourelle P, Lambowitz AM, Scott MS, Abou-Elela S. 2018. Simultaneous sequencing of coding and noncoding RNA reveals a human transcriptome dominated by a small number of highly expressed noncoding genes. *RNA N Y N* **24**: 950–965.

Bolger AM, Lohse M, Usadel B. 2014. Trimmomatic: a flexible trimmer for Illumina sequence data. *Bioinformatics* **30**: 2114–2120.

Bratkovič T, Božič J, Rogelj B. 2020. Functional diversity of small nucleolar RNAs. *Nucleic Acids Res* **48**: 1627–1651.

Chen C-L, Perasso R, Qu L-H, Amar L. 2007. Exploration of Pairing Constraints Identifies a 9 Base-pair Core within Box C/D snoRNA–rRNA Duplexes. *J Mol Biol* **369**: 771–783.

Dale RK, Pedersen BS, Quinlan AR. 2011. Pybedtools: a flexible Python library for manipulating genomic datasets and annotations. *Bioinforma Oxf Engl* **27**: 3423–3424.

Davis CA, Hitz BC, Sloan CA, Chan ET, Davidson JM, Gabdank I, Hilton JA, Jain K, Baymuradov UK, Narayanan AK, et al. 2018. The Encyclopedia of DNA elements (ENCODE): data portal update. *Nucleic Acids Res* **46**: D794–D801.

Deschamps-Francoeur G, Boivin V, Abou Elela S, Scott MS. 2019. CoCo: RNA-seq read assignment correction for nested genes and multimapped reads. *Bioinformatics* **35**: 5039–5047.

Deschamps-Francoeur G, Simoneau J, Scott MS. 2020. Handling multi-mapped reads in RNA-seq. *Comput Struct Biotechnol J* **18**: 1569–1576.

Dobin A, Davis CA, Schlesinger F, Drenkow J, Zaleski C, Jha S, Batut P, Chaisson M, Gingeras TR. 2013. STAR: ultrafast universal RNA-seq aligner. *Bioinformatics* **29**: 15–21.

Dupuis-Sandoval F, Poirier M, Scott MS. 2015. The emerging landscape of small nucleolar RNAs in cell biology. *Wiley Interdiscip Rev RNA* **6**: 381–397.

Elliott BA, Ho H-T, Ranganathan SV, Vangaveti S, Ilkayeva O, Assi HA, Choi AK, Agris PF, Holley CL. 2019. Modification of messenger RNA by 2′- O -methylation regulates gene expression in vivo. *Nat Commun* **10**: 1–9.

Fafard-Couture É, Bergeron D, Couture S, Abou-Elela S, Scott MS. 2021. Annotation of snoRNA abundance across human tissues reveals complex snoRNA-host gene relationships. *Genome Biol* **22**: 172.

Falaleeva M, Pages A, Matuszek Z, Hidmi S, Agranat-Tamir L, Korotkov K, Nevo Y, Eyras E, Sperling R, Stamm S. 2016. Dual function of C/D box small nucleolar RNAs in rRNA modification and alternative pre-mRNA splicing. *Proc Natl Acad Sci U S A* **113**: E1625–E1634.

Falaleeva M, Welden JR, Duncan MJ, Stamm S. 2017. C/D-box snoRNAs form methylating and non-methylating ribonucleoprotein complexes: Old dogs show new tricks. *BioEssays News Rev Mol Cell Dev Biol* **39**.

Fang X, Yang D, Luo H, Wu S, Dong W, Xiao J, Yuan S, Ni A, Zhang K-J, Liu X-Y, et al. 2017. SNORD126 promotes HCC and CRC cell growth by activating the PI3K–AKT pathway through FGFR2. *J Mol Cell Biol* **9**: 243–255.

Ganot P, Caizergues-Ferrer M, Kiss T. 1997. The family of box ACA small nucleolar RNAs is defined by an evolutionarily conserved secondary structure and ubiquitous sequence elements essential for RNA accumulation. *Genes Dev* **11**: 941–956.

Griffiths-Jones S, Bateman A, Marshall M, Khanna A, Eddy SR. 2003. Rfam: an RNA family database. *Nucleic Acids Res* **31**: 439–441.

Hebras J, Krogh N, Marty V, Nielsen H, Cavaillé J. 2019. Developmental changes of rRNA ribose methylations in the mouse. *RNA Biol* **17**: 150–164.

Howe KL, Achuthan P, Allen J, Allen J, Alvarez-Jarreta J, Amode MR, Armean IM, Azov AG, Bennett R, Bhai J, et al. 2021. Ensembl 2021. *Nucleic Acids Res* **49**: D884–D891.

Jorjani H, Kehr S, Jedlinski DJ, Gumienny R, Hertel J, Stadler PF, Zavolan M, Gruber AR. 2016. An updated human snoRNAome. *Nucleic Acids Res* **44**: 5068–5082.

Kehr S, Bartschat S, Stadler PF, Tafer H. 2011. PLEXY: efficient target prediction for box C/D snoRNAs. *Bioinformatics* **27**: 279–280.

Kishore S, Stamm S. 2006. The snoRNA HBII-52 Regulates Alternative Splicing of the Serotonin Receptor 2C. *Science* **311**: 230–232.

Kiss T. 2001. Small nucleolar RNA-guided post-transcriptional modification of cellular RNAs. *EMBO J* **20**: 3617–3622.

Kiss-László Z, Henry Y, Bachellerie J-P, Caizergues-Ferrer M, Kiss T. 1996. Site-Specific Ribose Methylation of Preribosomal RNA: A Novel Function for Small Nucleolar RNAs. *Cell* **85**: 1077–1088.

Leinonen R, Sugawara H, Shumway M. 2011. The Sequence Read Archive. *Nucleic Acids Res* **39**: D19–D21.

Lestrade L, Weber MJ. 2006. snoRNA-LBME-db, a comprehensive database of human H/ACA and C/D box snoRNAs. *Nucleic Acids Res* **34**: D158-162.

Li H, Handsaker B, Wysoker A, Fennell T, Ruan J, Homer N, Marth G, Abecasis G, Durbin R, 1000 Genome Project Data Processing Subgroup. 2009. The Sequence Alignment/Map format and SAMtools. *Bioinformatics* **25**: 2078–2079.

Lorenz R, Bernhart SH, Höner zu Siederdissen C, Tafer H, Flamm C, Stadler PF, Hofacker IL. 2011. ViennaRNA Package 2.0. *Algorithms Mol Biol AMB* **6**: 26.

Love MI, Huber W, Anders S. 2014. Moderated estimation of fold change and dispersion for RNA-seq data with DESeq2. *Genome Biol* **15**: 550.

Lu Z, Gong J, Zhang QC. 2018. PARIS: Psoralen Analysis of RNA Interactions and Structures with High Throughput and Resolution. *Methods Mol Biol Clifton NJ* **1649**: 59–84.

Lu Z, Zhang QC, Lee B, Flynn RA, Smith MA, Robinson JT, Davidovich C, Gooding AR, Goodrich KJ, Mattick JS, et al. 2016. RNA duplex map in living cells reveals higher order transcriptome structure. *Cell* **165**: 1267–1279.

Mann M, Wright PR, Backofen R. 2017. IntaRNA 2.0: enhanced and customizable prediction of RNA–RNA interactions. *Nucleic Acids Res* **45**: W435–W439.

Maxwell ES, Fournier MJ. 1995. The small nucleolar RNAs. *Annu Rev Biochem* **64**: 897–934.

O'Leary NA, Wright MW, Brister JR, Ciufo S, Haddad D, McVeigh R, Rajput B, Robbertse B, Smith-White B, Ako-Adjei D, et al. 2016. Reference sequence (RefSeq) database at NCBI: current status, taxonomic expansion, and functional annotation. *Nucleic Acids Res* **44**: D733-745.

Patterson DG, Roberts JT, King VM, Houserova D, Barnhill EC, Crucello A, Polska CJ, Brantley LW, Kaufman GC, Nguyen M, et al. 2017. Human snoRNA-93 is processed into a microRNA-like RNA that promotes breast cancer cell invasion. *NPJ Breast Cancer* **3**. https://www.ncbi.nlm.nih.gov/pmc/articles/PMC5503938/.

Pedregosa F, Varoquaux G, Gramfort A, Michel V, Thirion B, Grisel O, Blondel M, Prettenhofer P, Weiss R, Dubourg V, et al. 2011. Scikit-learn: Machine Learning in Python. *J Mach Learn Res* **12**: 2825–2830.

Quinlan AR, Hall IM. 2010. BEDTools: a flexible suite of utilities for comparing genomic features. *Bioinforma Oxf Engl* **26**: 841–842.

Raudvere U, Kolberg L, Kuzmin I, Arak T, Adler P, Peterson H, Vilo J. 2019. g:Profiler: a web server for functional enrichment analysis and conversions of gene lists (2019 update). *Nucleic Acids Res* **47**: W191–W198.

Schönberger B, Schaal C, Schäfer R, Voß B. 2018. RNA interactomics: recent advances and remaining challenges. *F1000Research* **7**: F1000 Faculty Rev-1824.

Scott MS, Ono M, Yamada K, Endo A, Barton GJ, Lamond AI. 2012. Human box C/D snoRNA processing conservation across multiple cell types. *Nucleic Acids Res* **40**: 3676–3688.

Sharma E, Sterne-Weiler T, O'Hanlon D, Blencowe BJ. 2016. Global Mapping of Human RNA-RNA Interactions. *Mol Cell* **62**: 618–626.

Sharma S, Yang J, van Nues R, Watzinger P, Kötter P, Lafontaine DLJ, Granneman S, Entian K-D. 2017. Specialized box C/D snoRNPs act as antisense guides to target RNA base acetylation. *PLoS Genet* **13**. https://www.ncbi.nlm.nih.gov/pmc/articles/PMC5464676/.

Van Nostrand EL, Freese P, Pratt GA, Wang X, Wei X, Xiao R, Blue SM, Chen J-Y, Cody NAL, Dominguez D, et al. 2020. A large-scale binding and functional map of human RNA-binding proteins. *Nature* **583**: 711–719.

Van Nostrand EL, Pratt GA, Shishkin AA, Gelboin-Burkhart C, Fang MY, Sundararaman B, Blue SM, Nguyen TB, Surka C, Elkins K, et al. 2016. Robust transcriptome-wide discovery of RNA-binding protein binding sites with enhanced CLIP (eCLIP). *Nat Methods* **13**: 508–514.

Vaquero-Garcia J, Barrera A, Gazzara MR, González-Vallinas J, Lahens NF, Hogenesch JB, Lynch KW, Barash Y. 2016. A new view of transcriptome complexity and regulation through the lens of local splicing variations. *eLife* **5**: e11752.

Vitali P, Basyuk E, Le Meur E, Bertrand E, Muscatelli F, Cavaillé J, Huttenhofer A. 2005. ADAR2-mediated editing of RNA substrates in the nucleolus is inhibited by C/D small nucleolar RNAs. *J Cell Biol* **169**: 745–753.

Weinstein LB, Steitz JA. 1999. Guided tours: from precursor snoRNA to functional snoRNP. *Curr Opin Cell Biol* **11**: 378–384.

Yang SL, DeFalco L, Anderson DE, Zhang Y, Aw JGA, Lim SY, Lim XN, Tan KY, Zhang T, Chawla T, et al. 2021. Comprehensive mapping of SARS-CoV-2 interactions in vivo reveals functional virus-host interactions. *Nat Commun* **12**: 5113.

Zhong F, Zhou N, Wu K, Guo Y, Tan W, Zhang H, Zhang X, Geng G, Pan T, Luo H, et al. 2015. A SnoRNA-derived piRNA interacts with human interleukin-4 pre-mRNA and induces its decay in nuclear exosomes. *Nucleic Acids Res* **43**: 10474–10491.

Zuker M. 2003. Mfold web server for nucleic acid folding and hybridization prediction. *Nucleic Acids Res* **31**: 3406–3415.

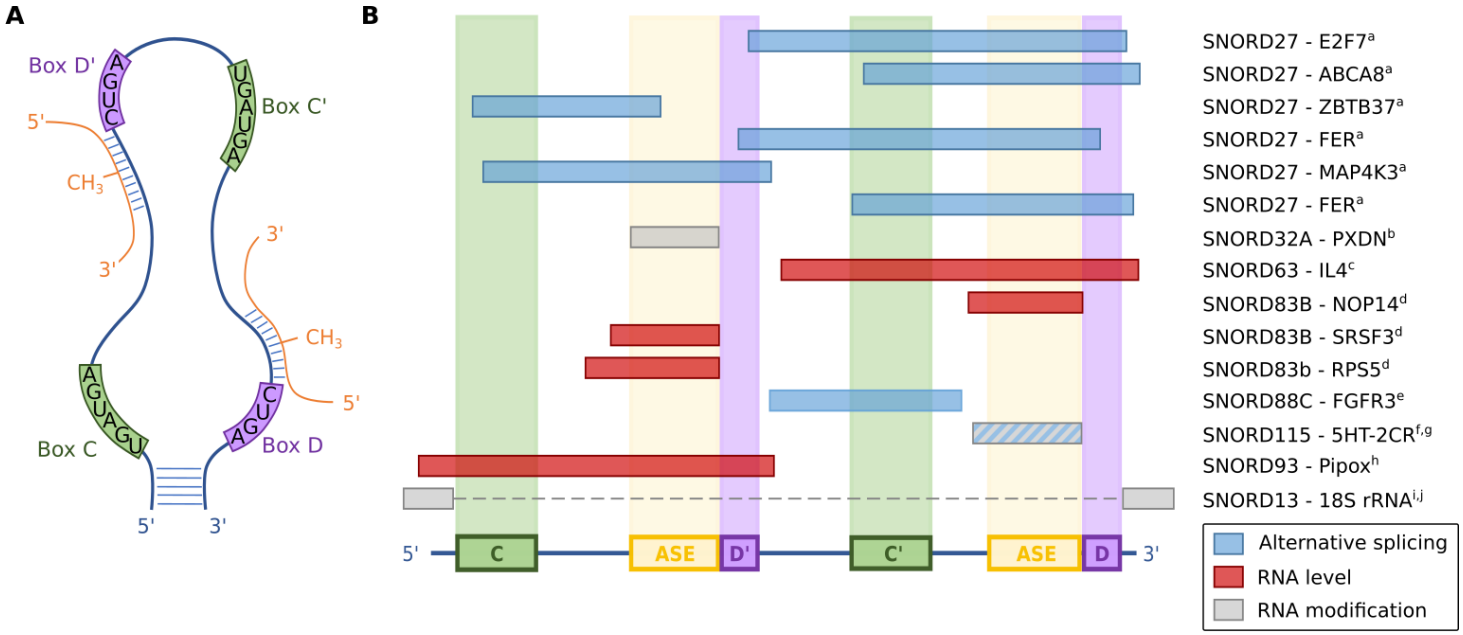
A
Box D'
Box C'
5'
CH3
3'
3'
CH3
5'
Box C
Box D
5'
3'
B
SNORD27 - E2F7a
SNORD27 - ABCA8a
SNORD27 - ZBTB37a
SNORD27 - FERa
SNORD27 - MAP4K3a
SNORD27 - FERa
SNORD32A - PXDNb
SNORD63 - IL4c
SNORD83B - NOP14d
SNORD83B - SRSF3d
SNORD83b - RPS5d
SNORD88C - FGFR3e
SNORD115 - 5HT-2CRf,g
SNORD93 - Pipoxh
SNORD13 - 18S rRNAi,j
5'
C
ASE
D'
C'
ASE
D
3'
Alternative splicing
RNA level
RNA modification

Figure 1

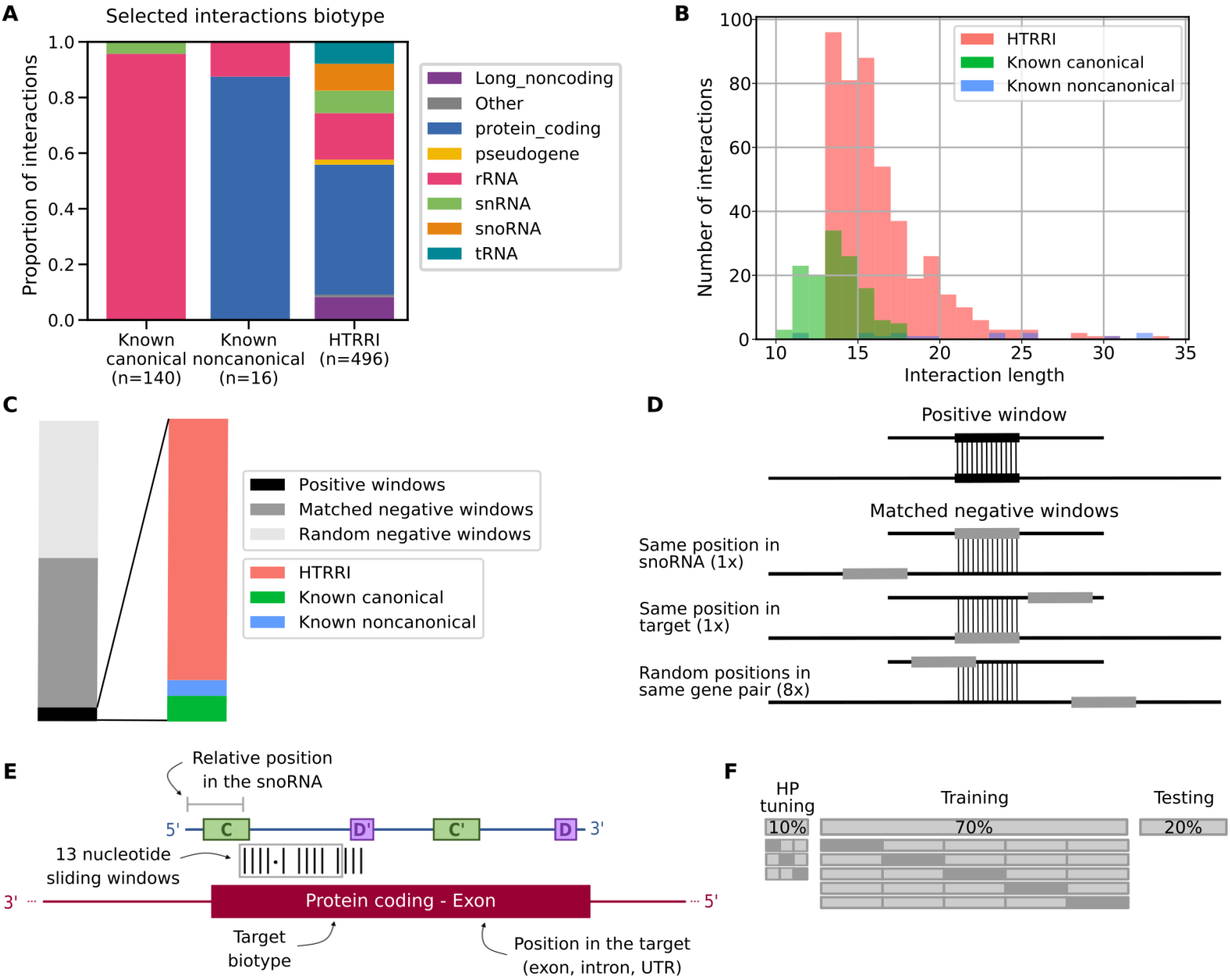
A
Selected interactions biotype
Proportion of interactions
1.0
0.8
0.6
0.4
0.2
0.0
Known canonical (n=140)
Known noncanonical (n=16)
HTRRI (n=496)
Long_noncoding
Other
protein_coding
pseudogene
rRNA
snRNA
snoRNA
tRNA
B
Number of interactions
100
80
60
40
20
0
10
15
20
25
30
35
Interaction length
HTRRI
Known canonical
Known noncanonical
C
Positive windows
Matched negative windows
Random negative windows
HTRRI
Known canonical
Known noncanonical
D
Positive window
Matched negative windows
Same position in snoRNA (1x)
Same position in target (1x)
Random positions in same gene pair (8x)
E
Relative position in the snoRNA
5'
C
D'
C'
D
3'
13 nucleotide sliding windows
3'
Protein coding - Exon
5'
Target biotype
Position in the target (exon, intron, UTR)
F
HP tuning
10%
Training
70%
Testing
20%

Figure 2

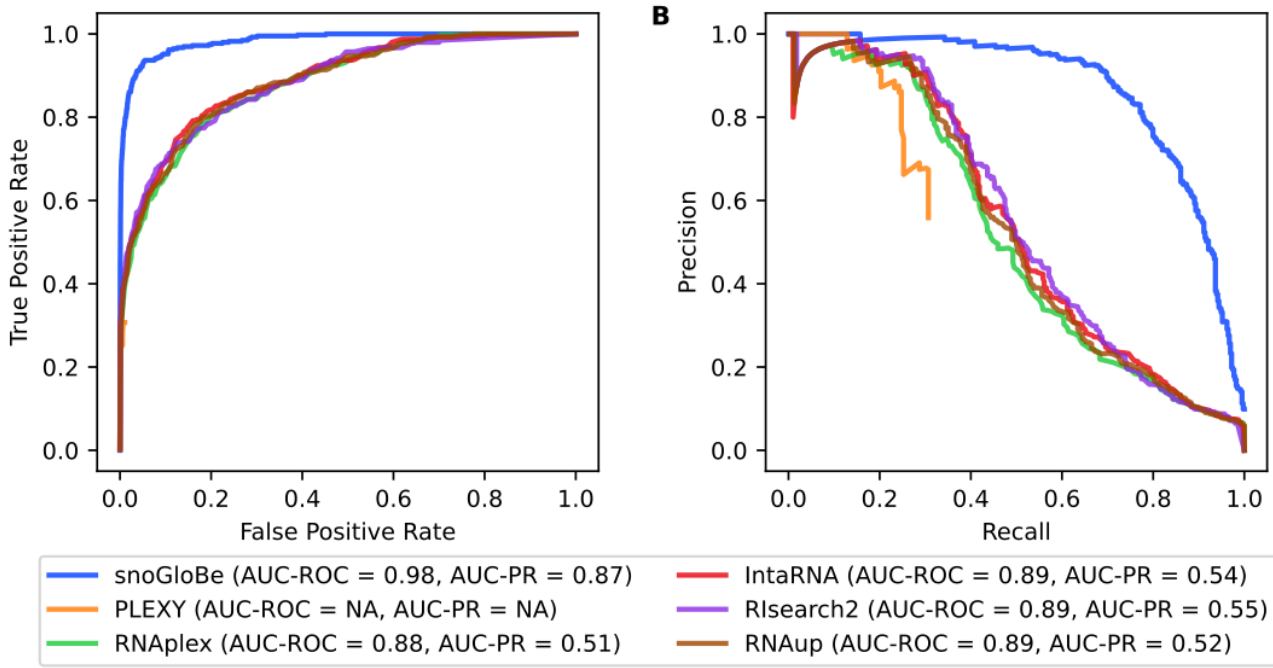

C

	snoGloBe	RNAplex	IntaRNA	RIsearch2	RNAup	PLEXY
Threshold used	0.503	-14.40	-13.51	-12.35	-13.87	-9.45
True positives (% of positives)	**275 (69.8)**	108 (27.4)	113 (28.7)	123 (31.2)	114 (28.9)	40 (19.9)
False positives (% of negatives)	30 (0.4)	12 (0.2)	12 (0.2)	14 (0.2)	13 (0.2)	**4 (0.1)**
False negatives (% of positives)	**119 (30.2)**	286 (72.6)	281 (71.3)	271 (68.8)	280 (71.1)	161 (80.1)
True negatives (% of negatives)	7910 (99.6)	7928 (99.8)	7928 (99.8)	7926 (99.8)	7927 (99.8)	**4643 (99.9)**
Matthews correlation coefficient	**0.78**	0.49	0.50	0.52	0.50	0.42
Accuracy	**0.98**	0.96	0.96	0.97	0.96	0.97
Precision	0.90	0.90	0.90	0.90	0.90	0.91
F1-score	**0.79**	0.42	0.44	0.46	0.44	0.33

D

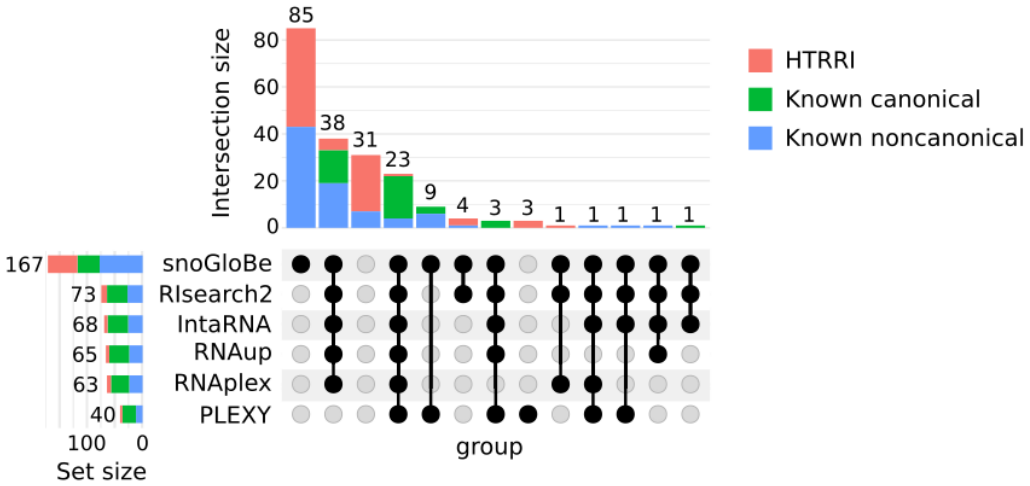

Figure 3

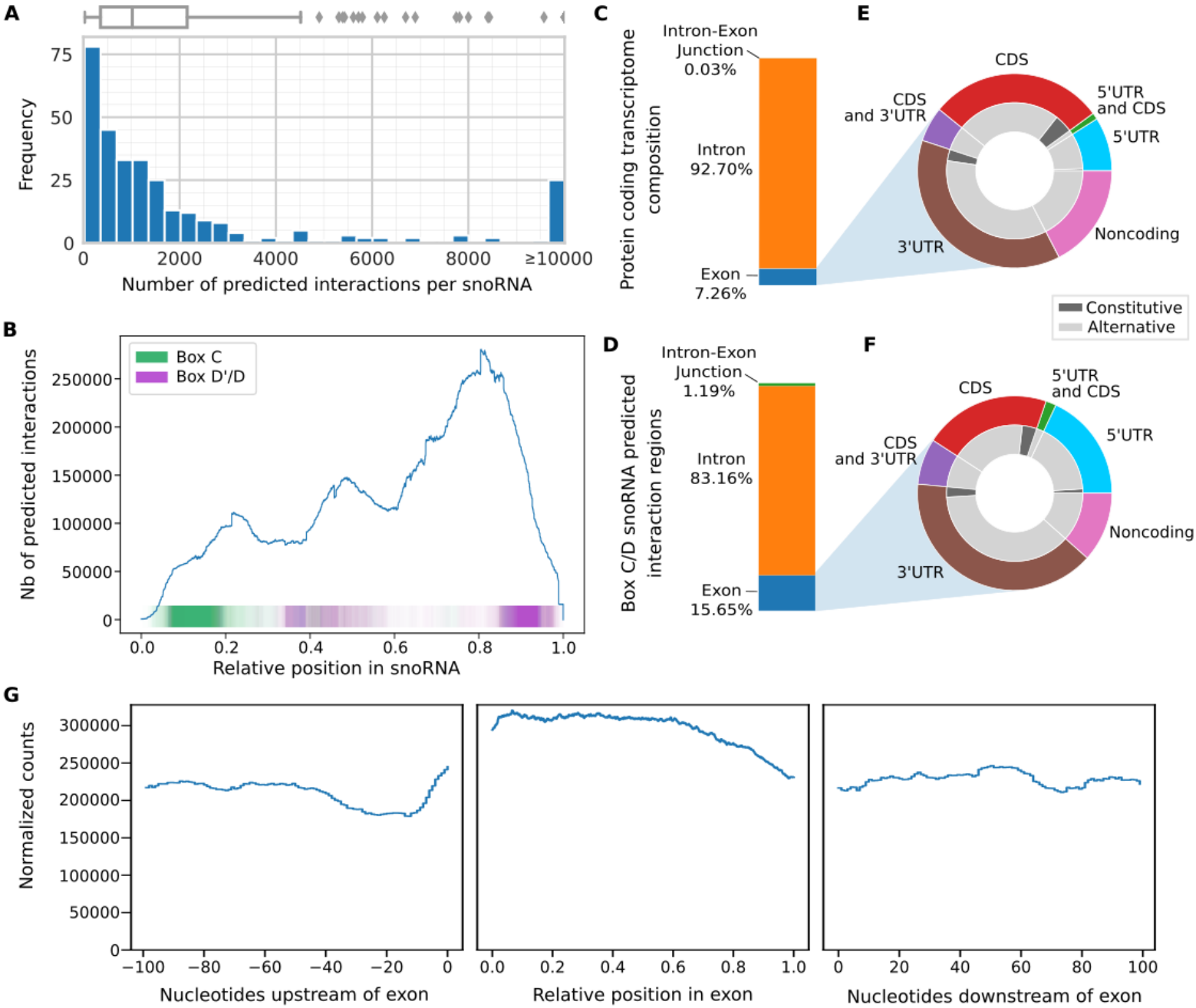
A
Frequency
Number of predicted interactions per snoRNA
B
Box C
Box D'/D
Nb of predicted interactions
Relative position in snoRNA
C
Protein coding transcriptome composition
Intron-Exon Junction 0.03%
Intron 92.70%
Exon 7.26%
D
Box C/D snoRNA predicted interaction regions
Intron-Exon Junction 1.19%
Intron 83.16%
Exon 15.65%
E
F
CDS
5'UTR and CDS
5'UTR
Noncoding
3'UTR
CDS and 3'UTR
Constitutive
Alternative
G
Normalized counts
Nucleotides upstream of exon
Relative position in exon
Nucleotides downstream of exon

Figure 4

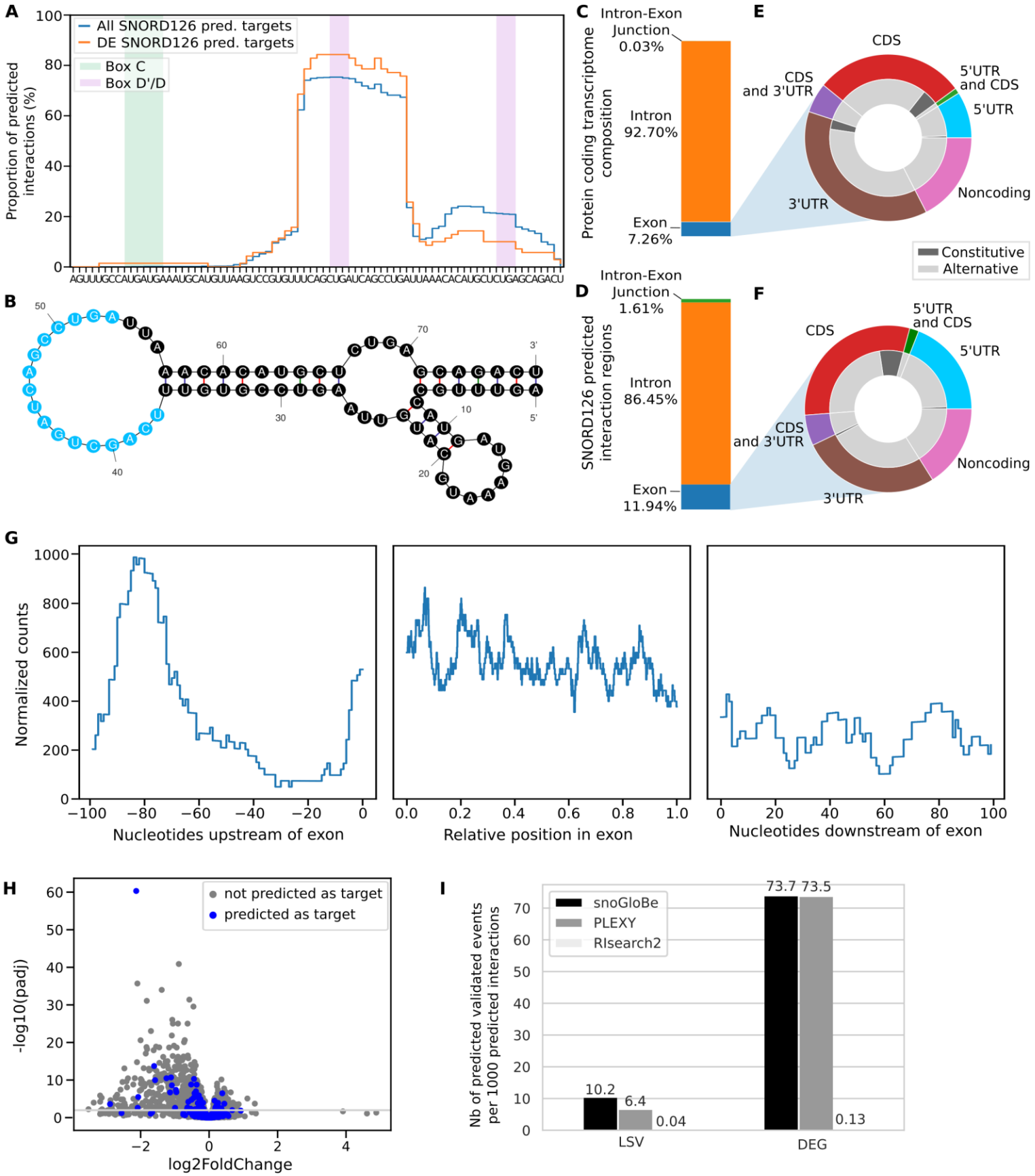
A
All SNORD126 pred. targets
DE SNORD126 pred. targets
Box C
Box D'/D
Proportion of predicted interactions (%)
AGUUUGCCAUGAUGAAAUGCAUGUUAAGUCCGUGUUUCAGCUGAUCAGCCUGAUUAAACACAUGCUCUGAGCAGACU
B
C
Intron-Exon Junction 0.03%
Intron 92.70%
Exon 7.26%
Protein coding transcriptome composition
E
CDS
5'UTR and CDS
5'UTR
Noncoding
3'UTR
CDS and 3'UTR
Constitutive
Alternative
D
Intron-Exon Junction 1.61%
Intron 86.45%
Exon 11.94%
SNORD126 predicted interaction regions
F
CDS
5'UTR and CDS
5'UTR
Noncoding
3'UTR
CDS and 3'UTR
G
Normalized counts
Nucleotides upstream of exon
Relative position in exon
Nucleotides downstream of exon
H
not predicted as target
predicted as target
-log10(padj)
log2FoldChange
I
snoGloBe
PLEXY
RIsearch2
Nb of predicted validated events per 1000 predicted interactions
10.2
6.4
0.04
73.7
73.5
0.13
LSV
DEG

Figure 5

A

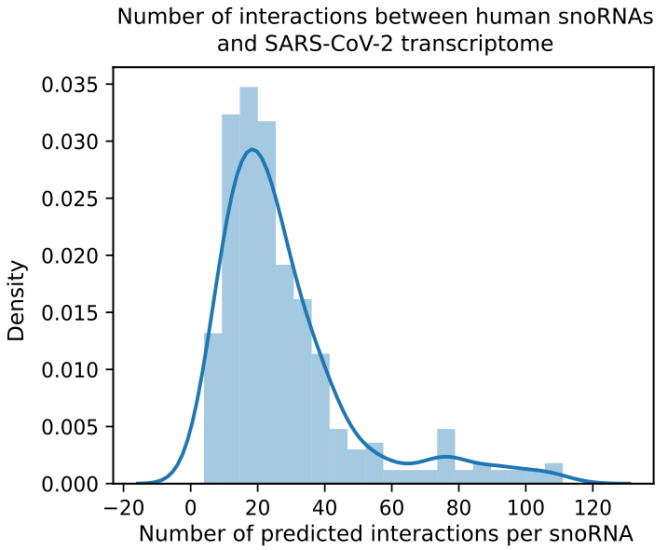
Number of interactions between human snoRNAs
and SARS-CoV-2 transcriptome
Density
0.035
0.030
0.025
0.020
0.015
0.010
0.005
0.000
−20
0
20
40
60
80
100
120
Number of predicted interactions per snoRNA

B

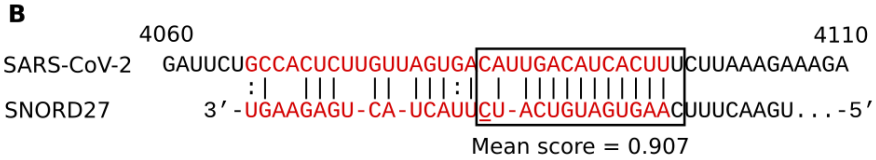
4060
4110
SARS-CoV-2 GAUUCUGCCACUCUUGUUAGUGACAUUGACAUCACUUUCUUAAAGAAAGA
:| ||| || |||:| | |||||||||||
SNORD27 3'-UGAAGAGU-CA-UCAUUCU-ACUGUAGUGAACUUUCAAGU...-5'
Mean score = 0.907

Figure 6

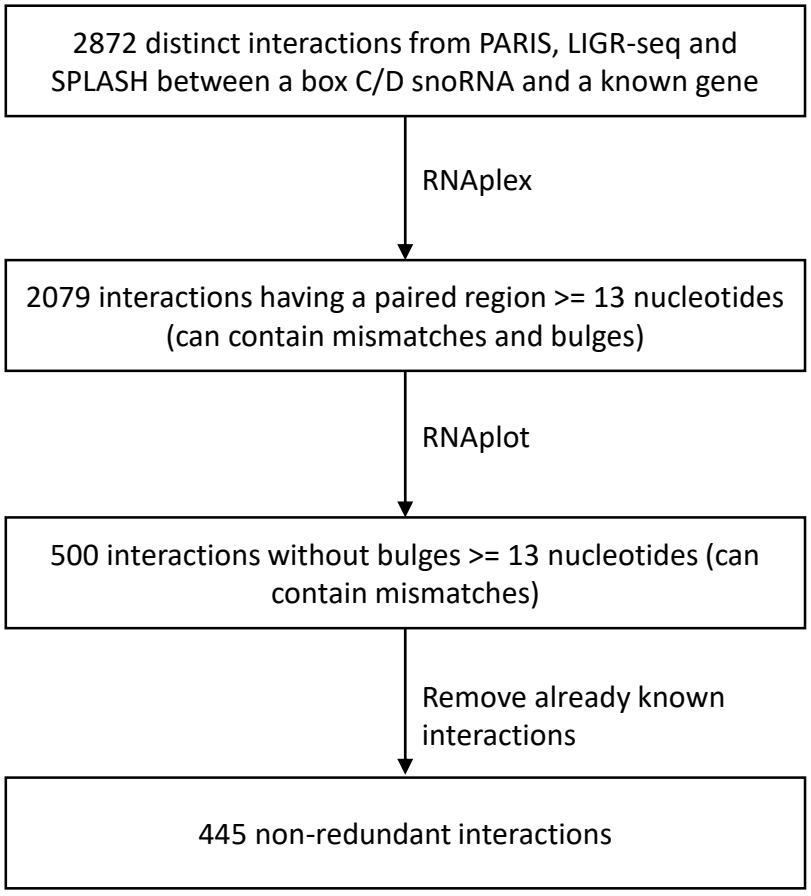

Figure S1: Overview of the filtering procedure starting with all distinct interactions detected in at least one HTRRI dataset involving a snoRNA to obtain the final HTRRI formatted datasets. The number of interactions remaining at each step is indicated.

Tool	Options used	Version	Ref
snoGloBe	-t 0.505	0.1.0	This paper
PLEXY	-e -9.29	N/A	Kehr et al., 2011
RNAplex	-e -14.51	2.4.14	Lorenz et al., 2011
RNAup	-e -13.97	2.4.14	Lorenz et al., 2011
RIsearch2	-e -12.49 -s 1	2.1	Alkan et al., 2017
IntaRNA	-e -13.30 --noSeed	3.1.1	Mann et al., 2017

Figure S2: List of tools compared for the prediction of C/D snoRNA-RNA interactions as well as their parameter values used, version and paper reference.

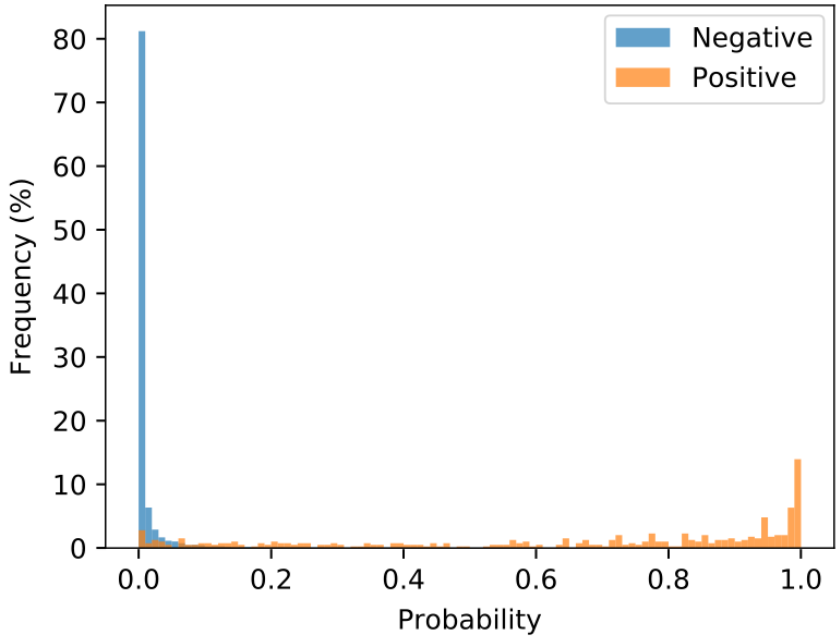

Figure S3: Distribution of the scores output by snoGloBe for the positive and negative examples in the test set.

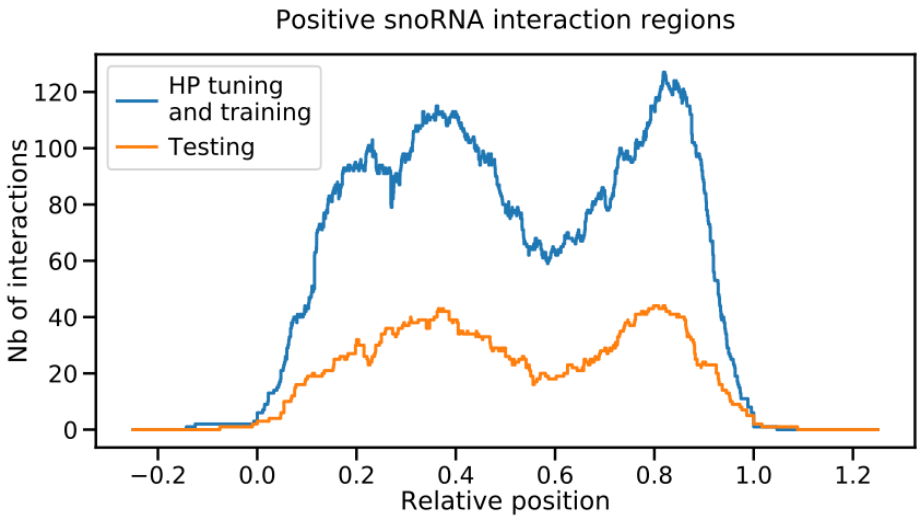

Figure S4: Profiles representing the number of predicted interactions from the hyperparameter tuning and training sets (blue) or the test set (orange) that involve specific positions in the snoRNA, for all snoRNAs considered simultaneously.

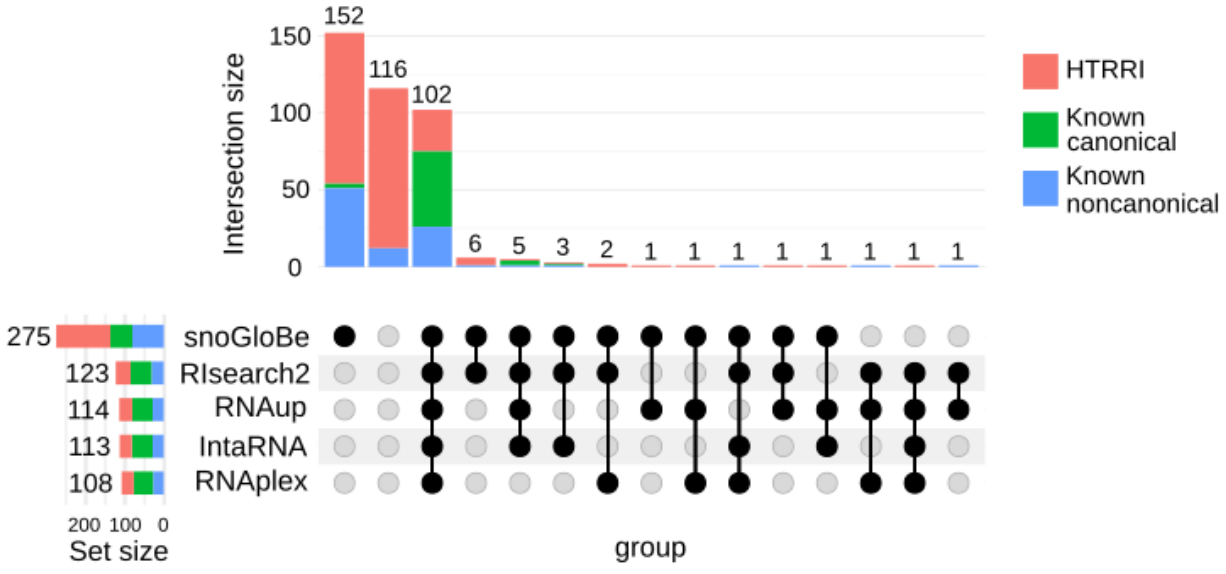

Figure S5: Upset plot indicating the number of correctly predicted interactions for all predictors compared, considering all the box C/D snoRNAs. The color legend on the right indicates the different interaction types. This figure differs from Figure 3D by showing the interactions from all the snoRNAs from the test set, whereas the Figure 3D only shows the snoRNAs that have non-degenerated boxes D and D', which are the snoRNAs that we used with PLEXY. Here, PLEXY is not shown.

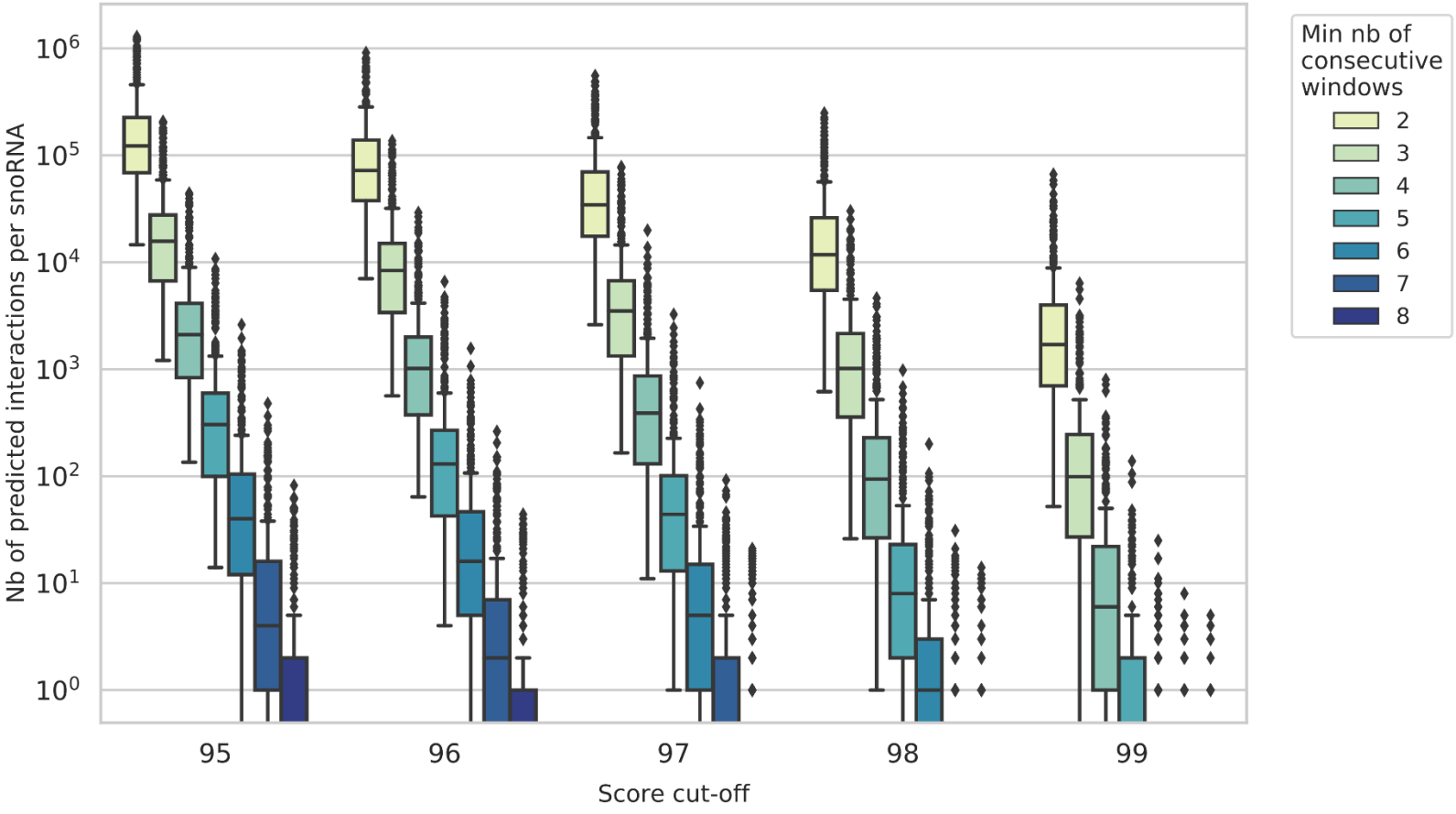

Figure S6: Boxplots depicting the distributions of the number of predicted interactions as a function of the parameter values used. The parameters considered are the number of predicted interactions per snoRNA (y axis), the score cut-off (x axis) and the minimum number of consecutive windows (different colors, with legend on the right).

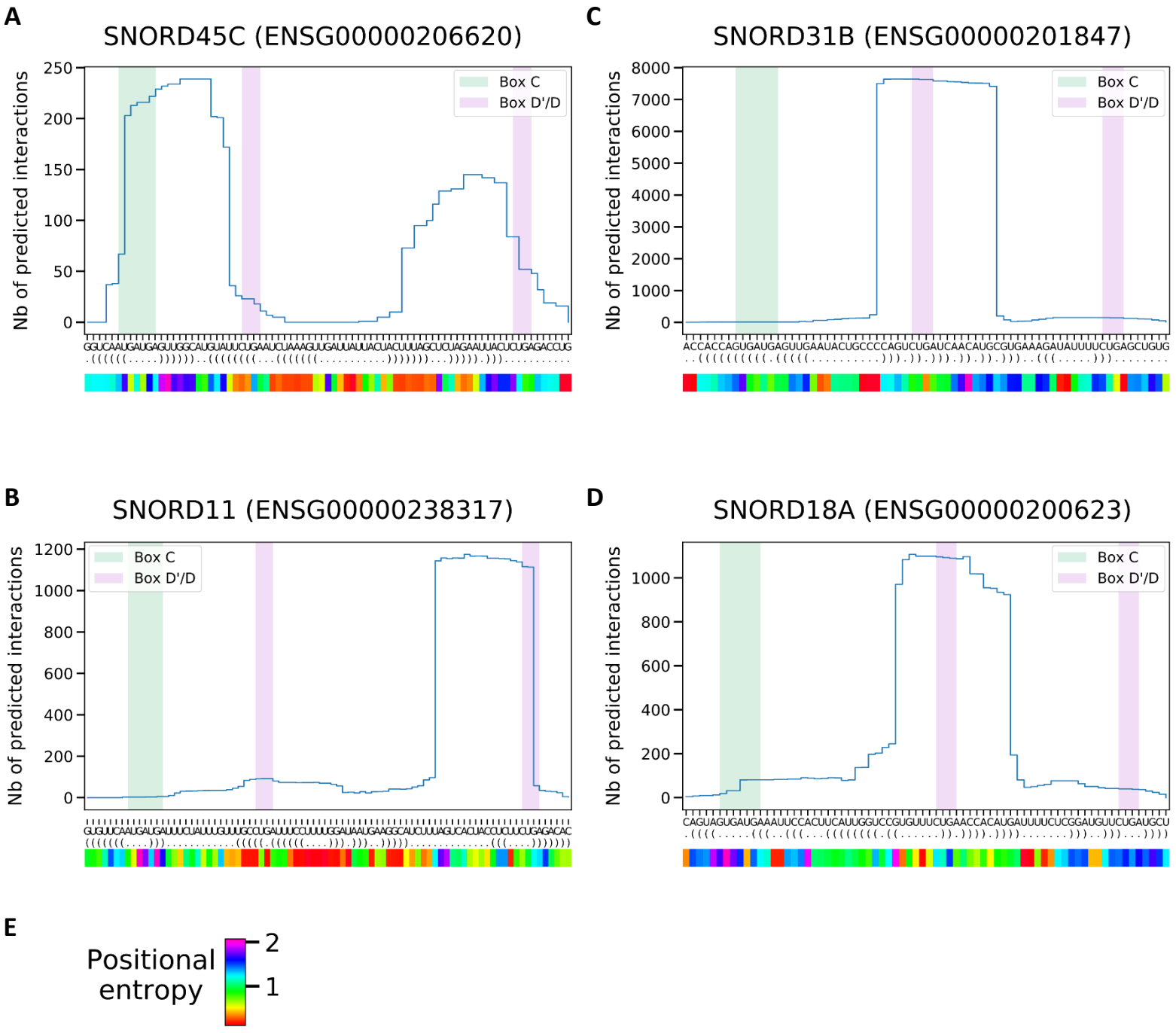

Figure S7: Profiles measuring the number of predicted interactions involving each position of the snoRNAs SNORD45C (A), SNORD11 (B), SNORD31B (C) and SNORD18A (D). The green and pink highlighting in the profiles represent respectively the positions of the C and D'/D boxes. The predicted folding of each snoRNA, as predicted by RNAplot, is shown using the dot-bracket format. The panel below each profile represents the positional entropy predicted by replot from the ViennaRNA package for each position of the snoRNA. The color legend for the position entropy score is given in E.

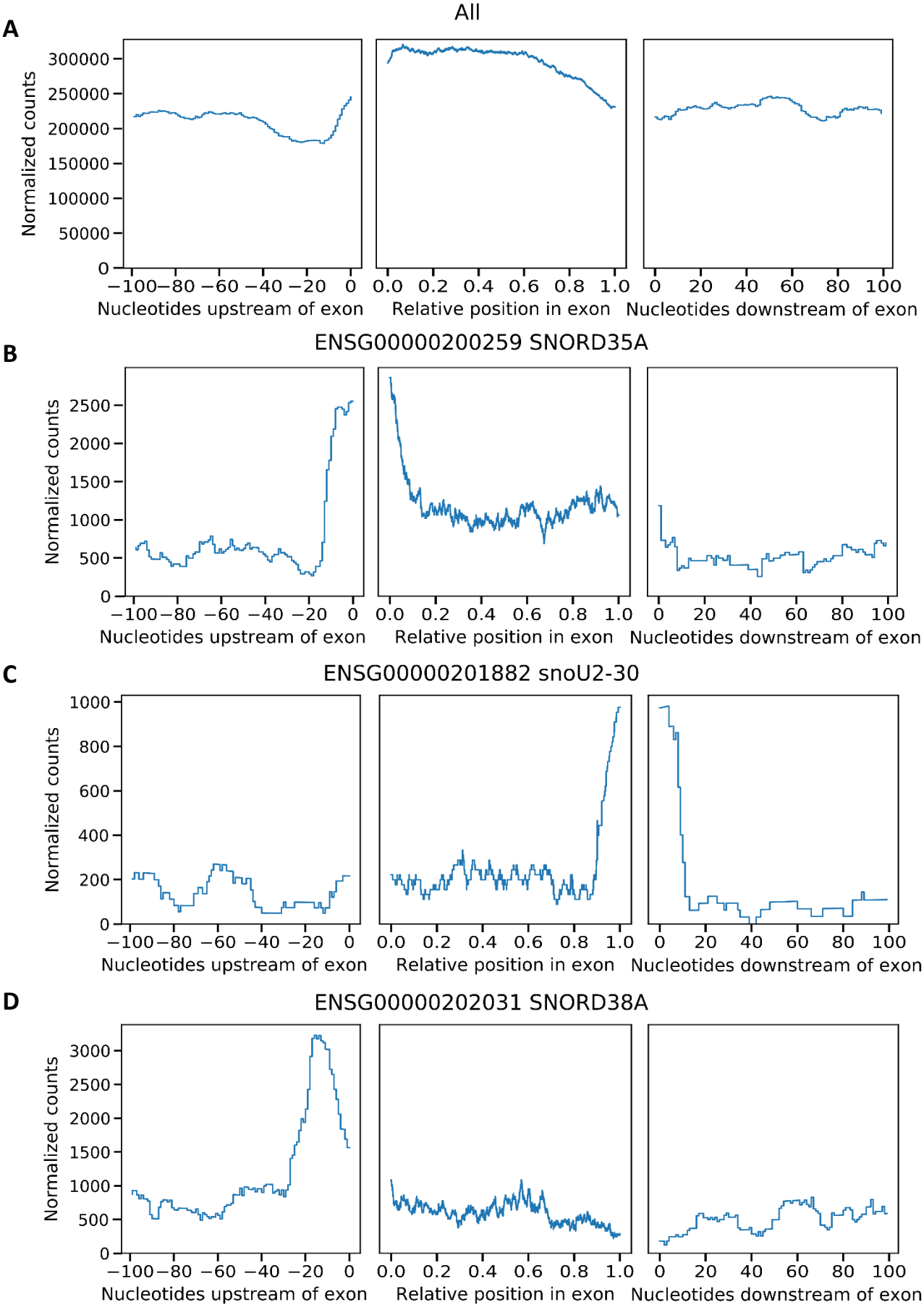

Figure S8: Profiles measuring the number of predicted interactions as a function of position with respect to the termini of introns and exons for all targets of all snoRNAs (A), SNORD35A (B), snoU2-30 (C) and SNORD38A (D).

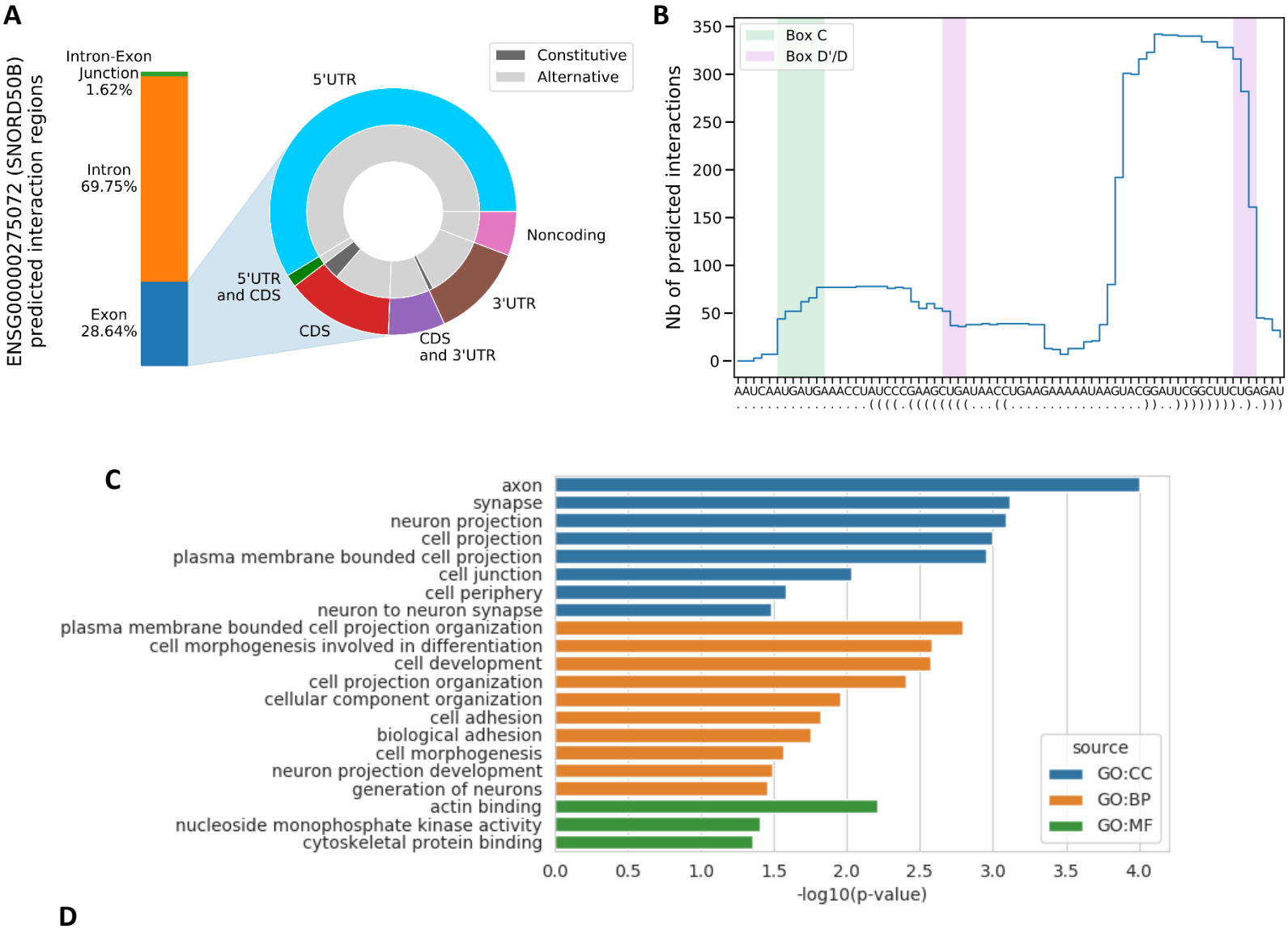

D

RBP	Number of predicted interactions overlapping binding sites	Significant target overlap (p-value < 10^{-5})	RBP binds snoRNA	snoRNA binds RBP pre-mRNA
DDX3X	43	X		
NCBP2	29	X	X	
GRWD1	25	X		X
BUD13	21	X	X	
FTO	19	X		X

Figure S9 SNORD50B displays a positional enrichment of binding on functionally related targets which are targeted by related RBPs. (A) SNORD50B targets are enriched in exons and more specifically in 5' UTRs compared to the transcriptome distribution (Fig. 4 C and E) as shown using a stacked bar plot showing the distribution of its targets across introns and exons (left) with a doughnut plot showing the breakdown for different exonic elements (right). (B) SNORD50B binds its targets using mainly its box D ASE, as shown with a positional profile measuring the number of targets each position of the snoRNA is predicted to bind. (C) SNORD50B predicted targets are enriched in specific gene ontology terms (CC: cellular component, BP: biological process, MF: molecular function) indicated using a horizontal bargraph. (D) SNORD50B displays strong association with specific RBPs. Table showing the number of predicted SNORD50B interactions that overlap binding sites for the indicated RBPs. (All 5 RBPs indicated have a significant overlap). In addition, 2 of the RBPs bind SNORD50B according to eCLIP experiments and SNORD50B is predicted to bind the pre-mRNA of 2 of the RBPs.

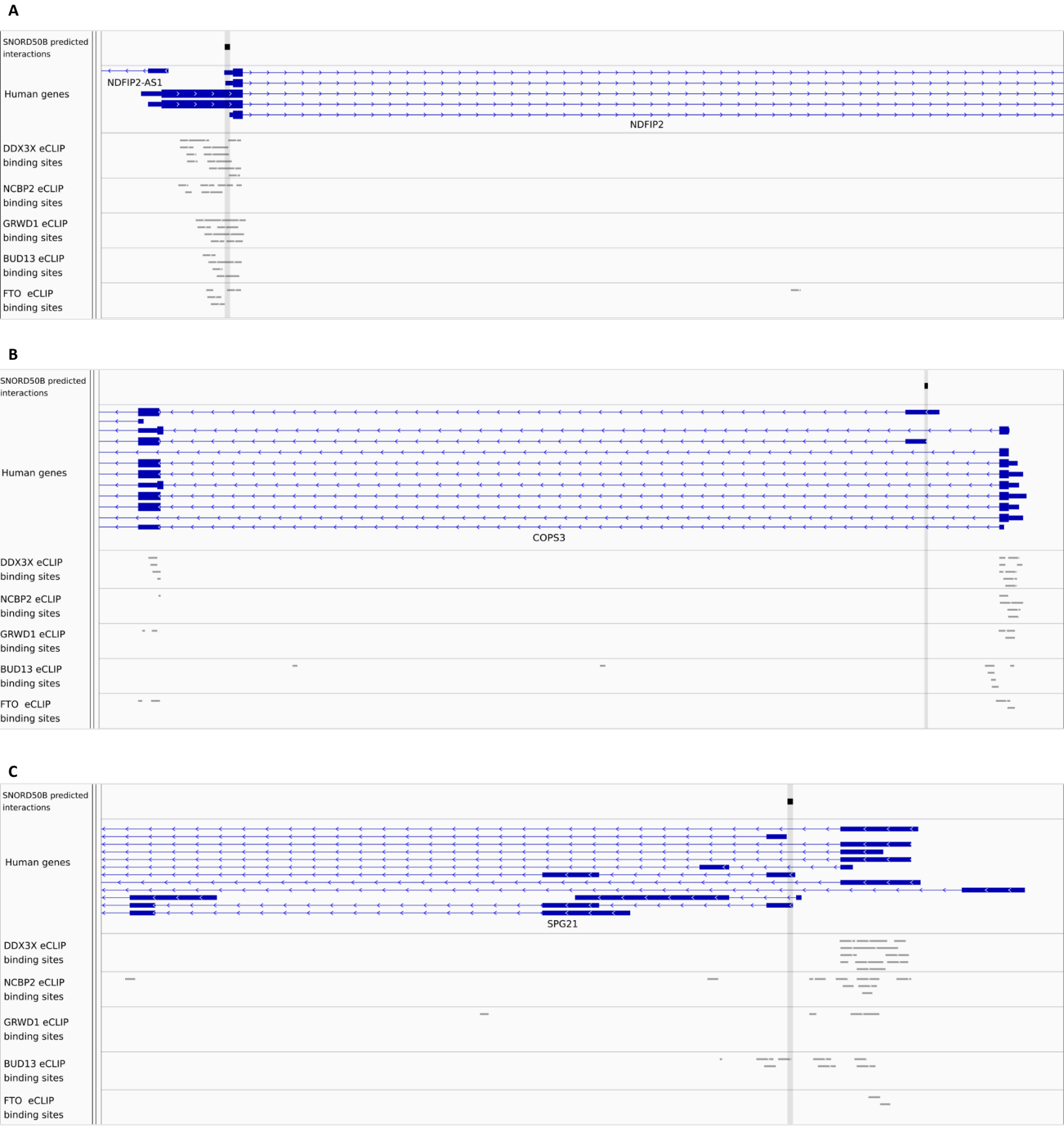

Figure S10 Examples of SNORD50B binding sites on alternative 5' UTRs. SNORD50B binding sites are enriched in 5' UTRs many of which are alternative including those in (A) NDIFP2, (B) COPS3 and (C) SPF21, as shown with genome browser screenshots. In each case, the top track displays the predicted binding position. The Human genes track indicates the architecture of the different isoforms encoded for these genes for the positional window chosen and the bottom tracks show the binding sites for the 5 RBPs indicated in Figure S9D according to ENCODE eCLIPs.

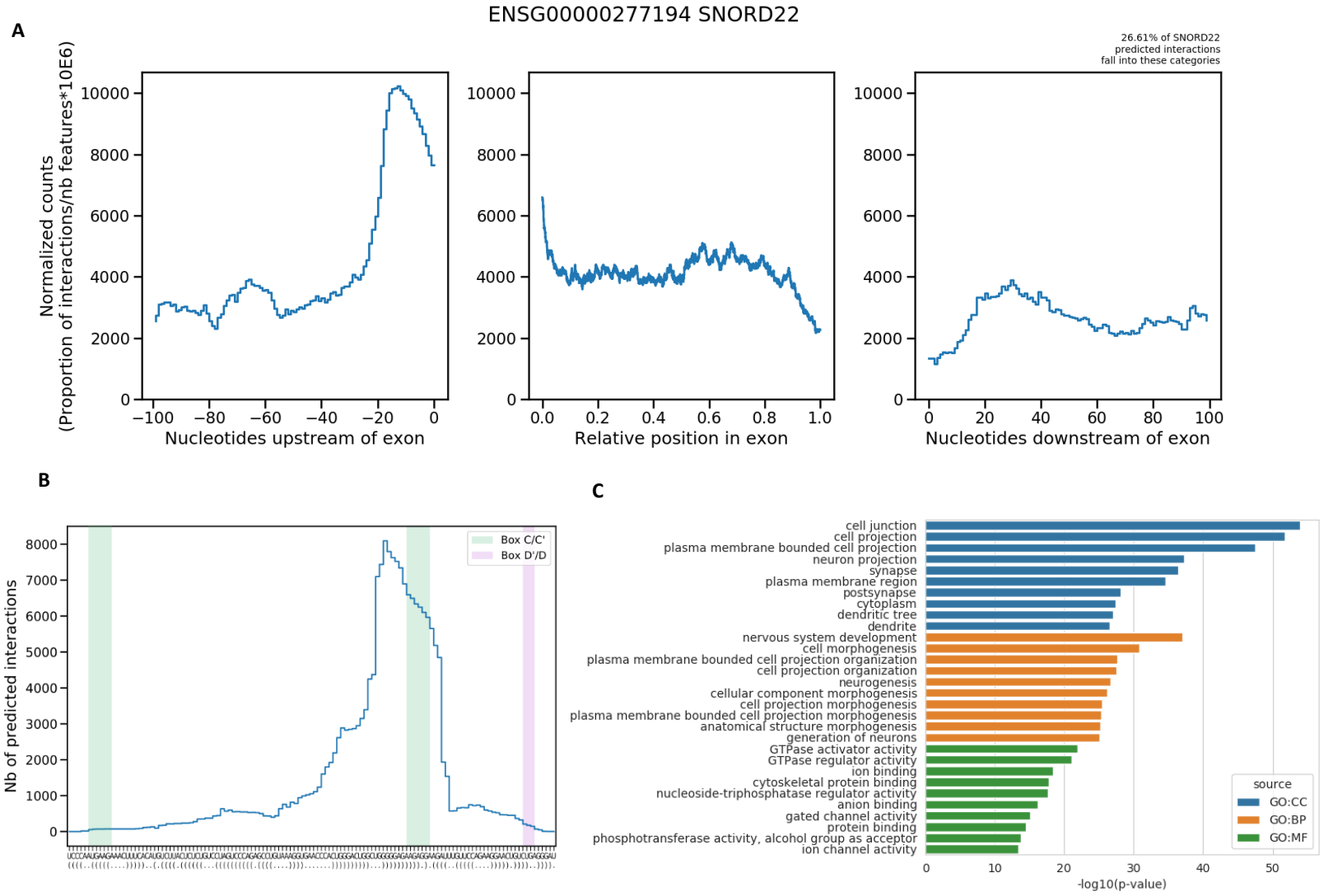

D

RBP	Number of predicted interactions overlapping binding sites	Significant target overlap (p-value < 10^{-5})	RBP binds snoRNA	snoRNA binds RBP pre-mRNA
PCBP2	363	X		
PTBP1	264	X	X	X
BUD13	256	X		
PRPF8	212	X	X	
AQR	207	X	X	

Figure S11 SNORD22 displays a positional enrichment of binding on functionally related targets which are targeted by related RBPs involved in splicing. (A) SNORD22 targets are enriched in 3' SSs of its targets as shown using a positional profile covering the last 100 nt of introns, the relative position in exons and the first 100 nt in introns. (B) SNORD22 binds its targets using a region overlapping its box C'. (C) SNORD22 predicted targets are enriched in specific gene ontology terms (CC: cellular component, BP: biological process, MF: molecular function) indicated using a horizontal bargraph. (D) SNORD22 displays strong association with specific RBPs. Table showing the number of predicted SNORD22 interactions that overlap binding sites for the indicated RBPs. (All 5 RBPs indicated have a significant overlap). In addition, 3 of the RBPs bind SNORD22 according to eCLIP experiments and SNORD22 is predicted to bind the pre-mRNA of 1 of the RBPs.

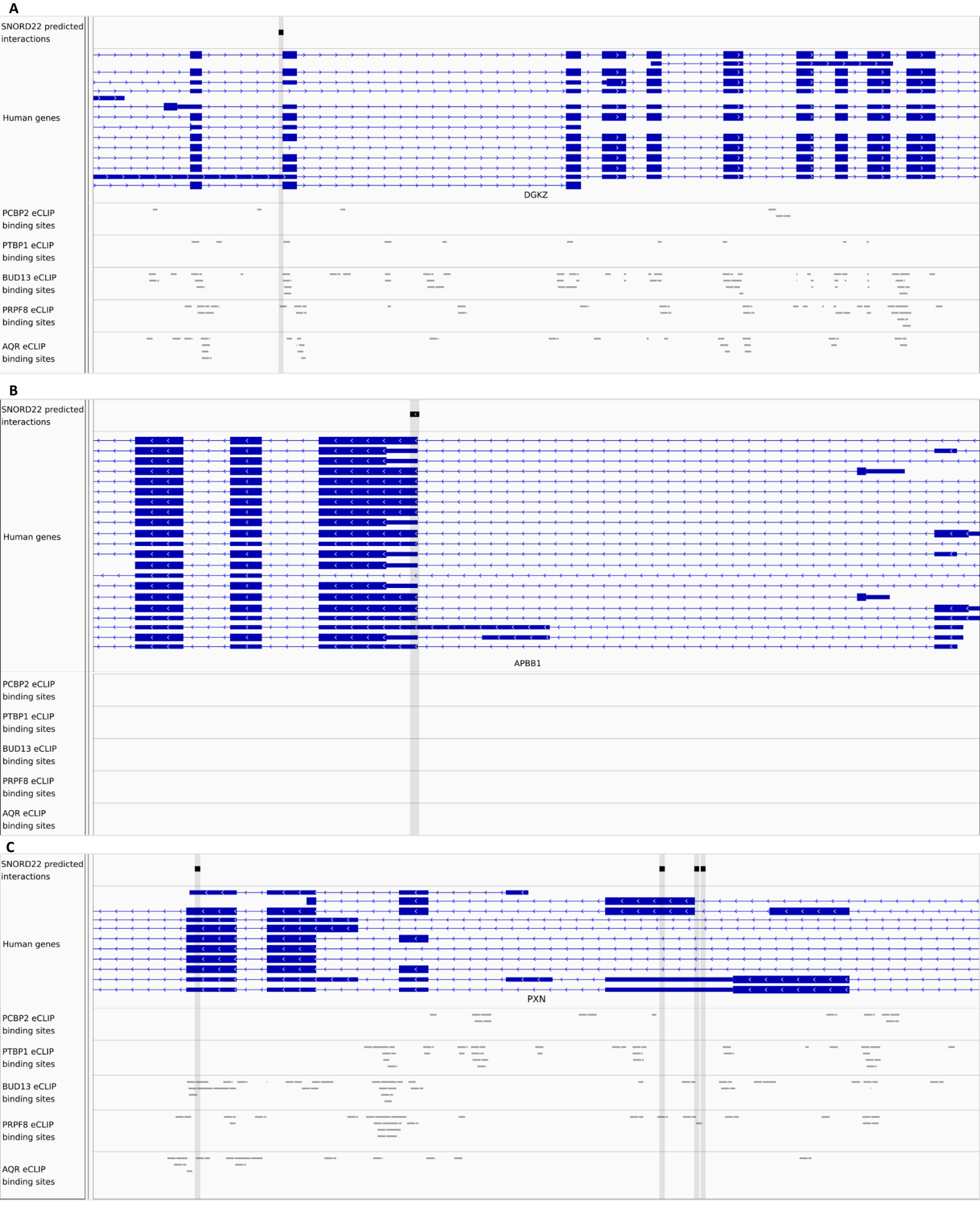

Figure S12 Examples of SNORD22 binding sites on alternative 3'SSs. SNORD22 binding sites are enriched in 3' SSs many of which are alternative including those in (A) DGKZ, (B) APBB1 and (C) PXN. Screenshots are as described in Figure S10.

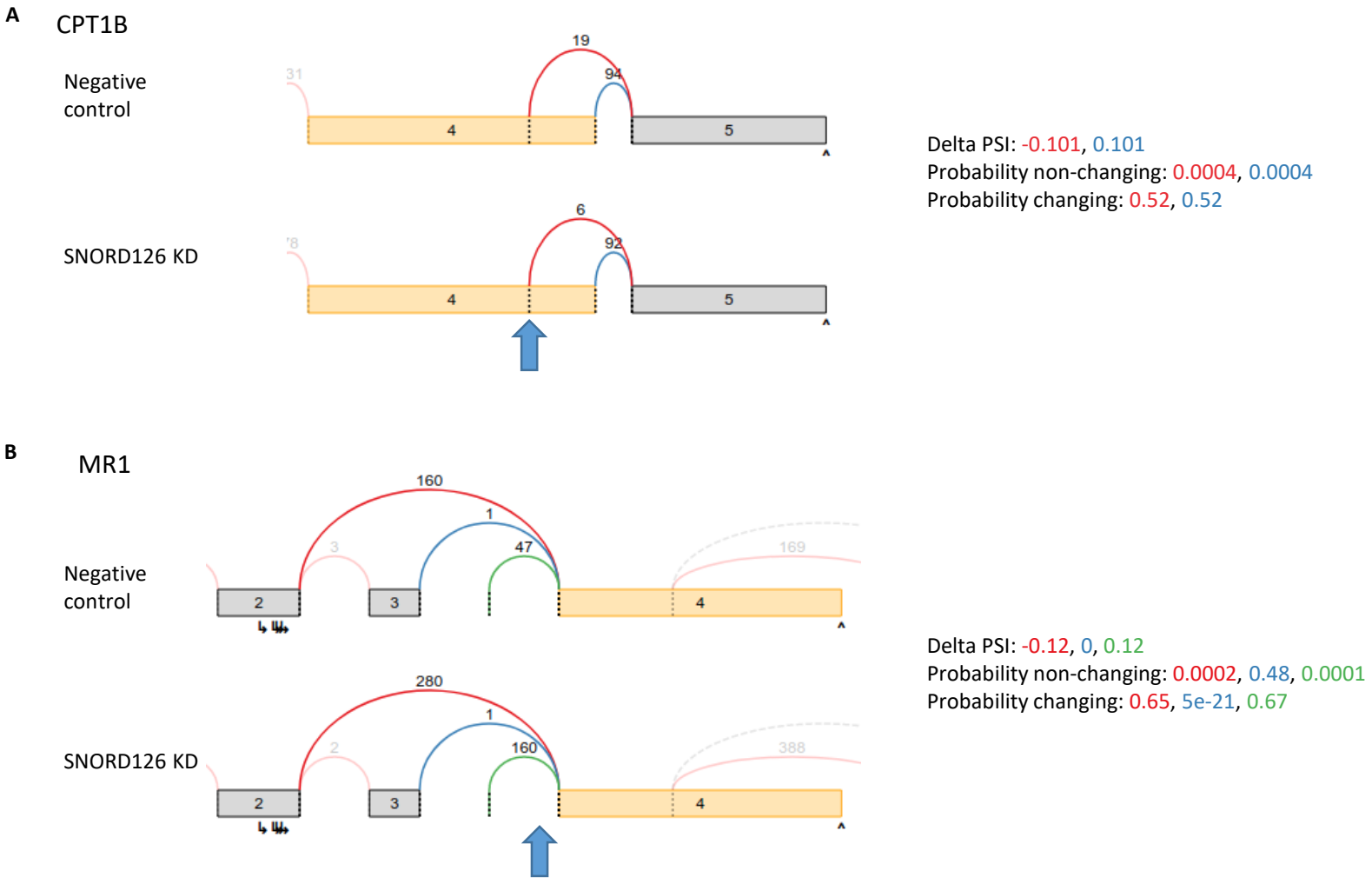

Figure S13: Examples of splicing events affected by the knockdown of SNORD126. Both CPT1B (A) and MR1 (B) display differential splicing following the knockdown (KD) of SNORD126 as shown using sashimi plots. The blue arrows represent the predicted interaction region. The colored arcs represent different splice junctions with the number of reads supporting them. Statistics of the splicing event are given on the right.

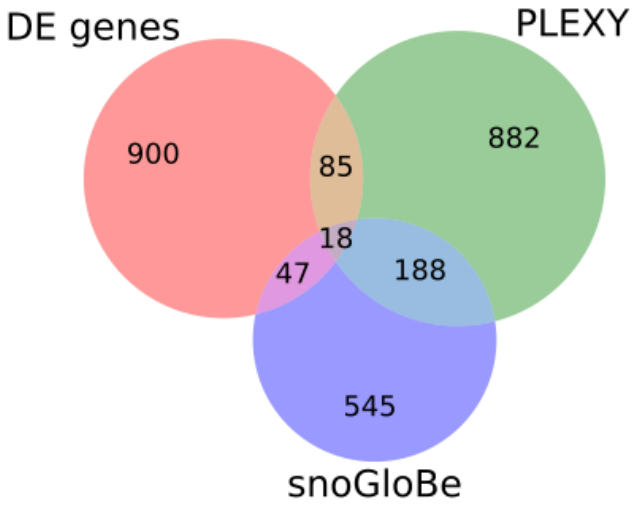

Figure S14: Overlap between the differentially expressed (DE) genes and the genes having at least one interaction predicted by PLEXY and/or snoGloBe.

ASO	Sequence
SNORD126_ASO1	5’-mC*mU*mG*mA*mA*A*C*A*C*G*G*A*C*T*T*mA*mA*mC*mA*mU*-3’
SNORD126_ASO2	5’-mA*mG*mC*mA*mU*G*T*G*T*T*T*A*A*T*C*mA*mG*mG*mC*mU*-3’
NC5	5’-mG*mC*mG*mA*mC*T*A*T*A*C*G*C*G*C*A*mA*mU*mA*mU*mG-3’

Figure S15: List of ASO sequences used for SNORD126 knockdown and negative control (NC5). * means phosphorothioate backbone, m means 2’-O-methoxyethyl.